MASTER THESIS IN SPACE PHYSICS

Energetic particle precipitation and polar surface air temperature variability

Joakim Kuven Osland
Supervisors: Hilde Nesse Tyssøy,
Kishore Kumar Grandhi & Yvan Orsolini

Abstract

Energetic Particle Precipitation (EPP) is known to have an impact on the chemical and thermal properties of the middle and upper atmosphere. Recent studies have also found ground level temperature anomalies in the polar regions in periods after high particle activity, with reductions in radiative cooling from ozone affecting the dynamics of the atmosphere.

Using the geomagnetic Ap-index as a proxy for EPP, the AO-index as a proxy for polar regional temperatures as well as MERRA-2 reanalysis temperature data, these signatures were investigated by finding correlation between the Ap- and AO-indices, and by dividing the years into high and low geomagnetic activity. The temperatures of low activity years and total climatology of the MERRA-2 data were subtracted from the high activity years, showing the temperature anomalies associated with EPP. The atmospheric conditions of the Sudden Stratospheric Warmings (SSW) and the Quasi-Biennial Oscillation (QBO) were taken into account to ensure our data was not biased towards their impacts. This was done at ground level (1000 hPa), in the lower troposphere (850 hPa), the middle stratosphere (10 hPa) and at the stratopause (1 hPa), to determine if signatures found were similar to those expected by the direct effect and dynamic response found by previous studies.

The stratopause levels (1 hPa, ~50 km) showed warm anomalies in-line with reduced radiative cooling from ozone, with cold anomalies in parts of the middle stratosphere (10 hPa, ~30 km) corresponding to a potential dynamic response. Ground level and lower troposphere showed warm anomalies above northern Europe and Siberia, with cold anomalies over North America and Greenland. This corresponds fairly well with the anomalies corresponding to positive AO-index, implying EPP may modulate the Arctic temperatures towards positive AO conditions, indicative of a strong polar vortex and reduced Brewer-Dobson circulation.

Acknowledgements

This thesis marks the end of my time as a student at the University of Bergen where I have spent the last few years working both on this master thesis and earning a certificate of education. I would like to thank my supervisors, Hilde Nesse Tyssøy, Kishore Kumar Grandhi and Yvan Orsolini, for sharing their expertise and technical knowledge as well as their patience, this thesis would not be possible if not for you pushing me when needed. Thanks to the rest of the Q3 team as well, for providing a good environment for a master student.

I would like to thank the other master students, in particular Roger, Bjørn, Kristian and Nini, with whom I have spent the last two years at UiB. Thanks for interesting talks, both related and completely unrelated to the work done, and for making the time spent memorable.

Thanks to my girlfriend Oda for being supportive and loving and for pushing me to do better.

A final thanks to the Birkeland Center of Space Science and the University of Bergen as a whole for giving me the opportunity to write this thesis. It has been exciting and enlightening, and I am very grateful.

For data used in this thesis, I thank

- *NOAA National Centers for Environmental Information* [a,c] for the Ap- and AO-indices.
- *NOAA Earth System Research Laboratory* for SSW data and *Freie Universität Berlin* for QBO data.
- *NASA Global Modeling and Assimilation Office (GMAO)* for MERRA-2 reanalysis data.

Joakim Kuven Osland
Bergen, June 2017

Contents

1 Introduction

1.1 Motivation

There is strong evidence that the current warming trend is related to man-made increase of the greenhouse gas levels. Many uncertainties remain, however, regarding the contribution of natural solar climate variability. In particular, recent studies suggest that the winter circulation patterns, such as the North Atlantic Oscillation or the Arctic Oscillation could be strongly modulated by solar variability. *Baldwin and Dunkerton* [2001] found indications that anomalous conditions in the stratosphere had ground level impacts. As it was known that changes in the solar output both in terms of radiative power and the solar wind led to chemical and thermal changes in the stratosphere, the impact of solar variability upon the surface of the Earth became a point of study. The mechanism proposed generally falls into two categories: Solar irradiance and Energetic Particle Precipitation. The latter is of particular interest as it for the first time will be part of the natural forcing included in the upcoming World Climate Research Program. Amongst others, *Rozanov et al.* [2005], *Seppälä et al.* [2009] and *Baumgaertner et al.* [2011] found temperature anomalies at polar regions as an effect from EPP. Since this is a fairly new field of study, uncertainties with regards to magnitude, geographical location and seasonal dependance are large and the associated mechanisms remain elusive.

Even though solar variability is not thought to have major effects globally, as noted by *Gray et al.* [2010], it may still have impacts locally, affecting temperatures, precipitation and winds in the lower atmosphere. A good understanding of the solar-driven climate change will help build better and more robust climate models which take solar effects into account. These models may be used to strengthen our understanding of anthropogenic climate change, which is one of the major problems humanity faces in our time.

1.2 Objectives

The objectives of this thesis is to investigate the effects of EPP on the polar winter climate. Using proxies for EPP and polar ground level temperatures as well as reanalysis temperature data, we seek to answer the following questions:

- What is the magnitude and geographical location of the effects, if any, of EPP on the polar winter climate?
- What is the time lag between the impact of EPP and the polar surface temperature response?
- Is the efficiency of the process dependent on background atmospheric conditions such as sudden stratospheric warmings or the phase of the quasi-biennial oscillation?

By answering these questions, we intend to strengthen the understanding of solar-driven climate change, thus contributing to a more complete understanding of the anthropogenic climate change.

2 Theory

It is general consensus that solar variability cannot account for the observed global warming throughout the last century. There are, on the other hand, large uncertainties associated with the natural climate variability. In particular, recent studies suggest that winter circulation patterns such as the North Atlantic Oscillation, over the Atlantic-European region could be strongly modulated by solar variability [*Gray et al.*, 2010, *Seppälä et al.*, 2014]. The following chapter describes the solar variability with respect to both electromagnetic and particle radiation. it gives a short introduction to the atmosphere and relevant processes. Finally, it addresses the proposed mechanisms to explain the climate response to variations in solar activity.

2.1 The sun and near earth

Our sun is a star approximately halfway through its life span with a surface temperature of about 6000 K. The radiation from the sun is the basis for the energy balance of Earth's climate and most life owes its existence to it. It is known to be a variable star on a monthly, decadal and millenial scale, both in terms of electromagnetic power and ejection of solar matter. We use several indices to quantify the solar activity. These could be measureable such as the radio flux or created by algorithms such as the sunspot number. It is also possible to measure the activity indirectly by looking at disturbances upon Earth's magnetic field with geomagnetic indices such as the Ap-index [*Usoskin*, 2017].

2.1.1 The Solar Cycle

An approximate 11-year cycle known as the *solar cycle* or the *solar magnetic cycle* is the time it takes for the solar magnetic field to change its polarity. At the peak of each solar cycle, the inner magnetic dynamo of the sun re-organizes. There are several indices used to represent the solar cycle such as sunspot number, F10.7 solar flux, Mg-ii-index and open solar flux (shown in Figure 2.1 b-e, respectively).

The sunspot is a visual manifestation, dark areas on the solar disc characterized by a strong

magnetic field that leads to a lower temperature (about 4000 K compared to 5800 K in the photosphere) [*Usoskin*, 2017]. The solar cycle has been observed for hundreds of years due to the very noticeble changes in sunspots, with several large sunspots observed during solar maximum while the number of sunspots can be close to zero during solar minimum as is shown in Figure 2.1a). Sunspots are often found in groups, making it difficult to measure each individually. The sunspot number is therefore calculated by combining the groups and individual sunspots. So sunspot number is a synthetic, rather than a physical, index. In general, it is noted as R. There are different algorithms to calculate the sunspot number. Figure 2.1b shows the *International Sunspot Number* as an index of the solar cycle. Figure 2.1c) and d) show alternate solar cycle indices such as the F10.7 index and the Mg-ii index. These are measured indices of the 10.7 cm radio emissions from the sun and solar UV-variability, respectively. These are not directly connected to the sunspot numbers [*Usoskin*, 2017]. In addition to sunspots, hotter regions called faculae are present on the solar disc. These are brighter than the surroundings and counter the dimming effect from the sunspots, giving a slight increase in total solar irradiance during solar maximum that leads to another measure of the solar cycle (Figure 2.1g)). The faculae are smaller than the sunspots, but more numerous and spread out. This means that sunspots are visible in the rotational period of the sun, but the changes in luminosity from the faculae are only visible over the solar cycle [*Gray et al.*, 2010].

In addition to the electromagnetic radiation, the sun emits particles as well. This constant stream of particles is referred to as the *solar wind*. The particle flux can be measured in situ with satellites, or with indices measuring their impact on Earth's magnetic field, such as the Ap-index shown in Figure 2.1h). The particle fluxes from the sun are more variable in their nature varying greatly over short time spans. However, a trend similar to the solar cycle is evident. The highest Ap values are not seen during solar maximum, however, but rather lagged a few years, peaking in the declining phase of the solar cycle [*Gray et al.*, 2010].

Particle radiation from extrasolar sources, so-called *galactic cosmic rays*, are highly energetic particles also visible on earth. During periods of strong solar wind the earth is partly shielded from these particles, causing a dip in their intensity. This means that even radiation from outside the solar system will have a noticeable variability with the solar cycle, as shown in Figure 2.1f) [*Gray et al.*, 2010].

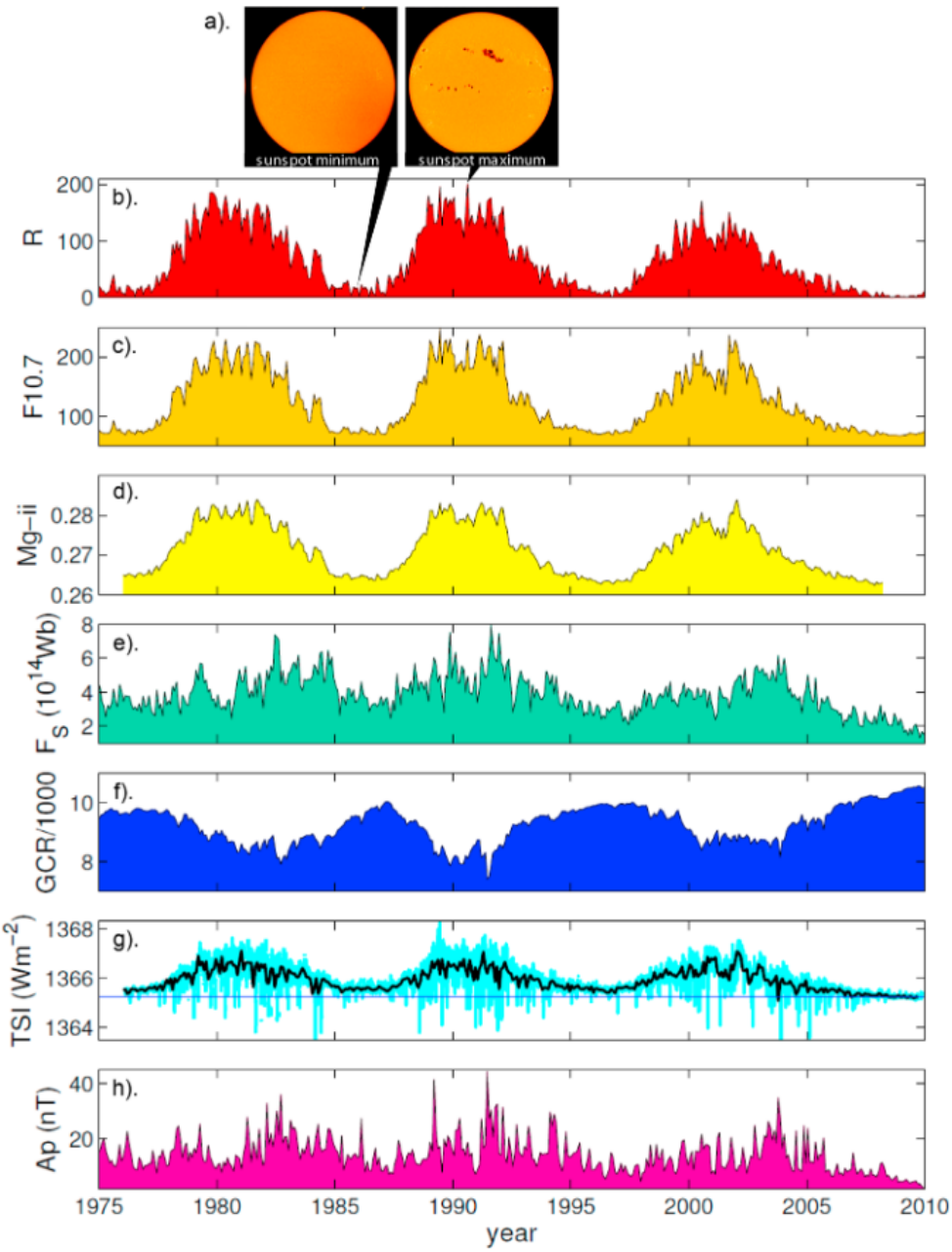

Figure 2.1: Different ways of measuring the solar cycle: a) images of the sun during solar minimum and maximum, respectively, b) the International Sunspot number R, c) F10.7-index, a measure of radio wave activity from the sun, d) Mg-ii-index, a measure of UV irradiance, e) The open solar flux F_s, a measure of particle activity, f) Galactic cosmic ray counts, anti-correlated with solar cycle, g) Total solar irradiance composite from observations, h) The geomagnetic Ap-index. Figure from *Gray et al.* [2010]

.

2.1.2 Total Solar Irradiance and spectral irradiance

As mentioned earlier, the total solar irradiance is increased during solar maximum due to the faculae countering the dimming from the sun spots. Figure 2.2 illustrates solar irradiance and its variance over the solar cycle. The total net increase is less than 1%, considered to be too low a variability to influence the climate globally [*Gray et al.*, 2010]. However, it still could affect locally due to increased evaporation and temperature changes, as will be shown in Chapter 2.3. In addition, the irradiance spectrum show differences over solar period. Although UV-radiation is a small part of the total irradiance it has a much larger variance, around 5%, and may as such have a greater influence. The middle part of Figure 2.2 shows a representation of how deep the different wavelengths penetrate the atmosphere; Low energy photons are much more likely to reach the surface while high energy UV-photons are generally absorbed higher up. At short wavelengths below 100 nm variations of up to 100% are observed, and signatures of this is visible between 500-1000 km above the earth, with temperature changes of up to 1000 K [*Gray et al.*, 2010].

2.1.3 The solar wind

As mentioned earlier, the geomagnetic Ap-index varies with the solar cycle with a 3-4 year lag. In the declining phase of the solar cycle plasma is released to the solar wind in bursts, called *Coronal Mass Ejections* (CME). The more widely known *solar flares* are often connected with these ejections as well. In addition, less violent releases of high-speed plasma from so-called *coronal holes*, open magnetic field lines on the Sun, giving a more constant boost to the solar wind. These holes are more long-lived than the CMEs, and recent work by amongst others *Asikainen and Ruopsa* [2016] have discussed their respective effects upon Earth. According to *Seppälä et al.* [2014], there has been a shift in the focus of studies of these events. Where before one mostly looked at CMEs, one now consider these an extreme event and look on the effects of constant particle precipitation or the effects of both. Although the solar irradiance is almost constant, the particle flux is more event-based and more inherently variable, but typically more common during the declining solar cycle.

The solar wind is a highly conductive plasma made up of electrons, hydrogen and helium ions, and thus carries with it its magnetic field. This is referred to as the *Interplanetary Mag-*

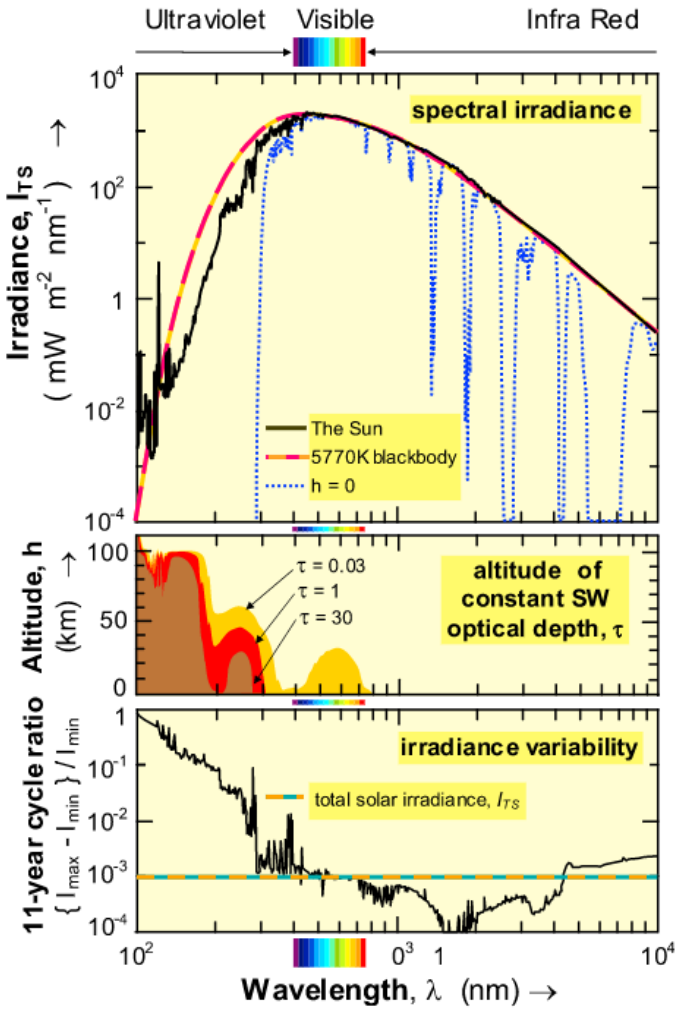

Figure 2.2: Top: Spectrum of solar irradiance (black line) compared to blackbody (red/yellow line). Blue dotted line shows radiation reaching Earths surface. Middle: Indication of how deep radiation penetrates into the atmosphere. Bottom: The spectral variance of solar irradiance over the solar period. Figure from *Gray et al.* [2010]

netic Field (IMF). When the IMF hits earth's magnetosphere, a bow shock is created where the solar wind is travelling past earth. This boundary region is called the *magnetopause*. When the magnetic field lines of the IMF are opposite of the ones around earth, magnetic reconnection occurs. The IMF and Earth's magnetic fields are connected and dragged downstream with the solar wind. This changes the shape of earth's magnetic field into a slightly flattened half-sphere facing the sun and giving it a long tail (the magnetotail) away

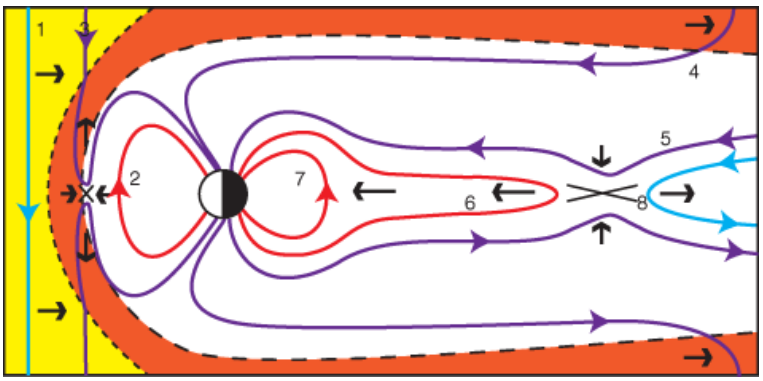

Figure 2.3: Schematic view of the Dungey cycle: Southward IMF (1) reconnecting with earths magnetosphere (2), creating open field lines (3) pulled away from the sun (4) and reconnecting on the nightside (5), pulling trapped plasma towards earth (6) and normalising the magnetic field line (7) before the process starts over. Plasma is also deposited downstream from the earth (8). From *Eastwood et al.* [2015]

from it. The tail might reconnect with the other end of the earth magnetic field, and travel back towards the earth. This causes plasma to be caught in the magnetosphere, which may in turn penetrate the upper atmosphere depending on magnetospheric acceleration and scattering processes. Note that because the particles follow the magnetic fields, their impact is generally seen close to the magnetic poles in what is referred to as the *auroral oval*. This causes the well known aurora borealis and australis. This cycle is called the *Dungey cycle* after Jim Dungey who first proposed it in 1961. A schematic view of the process is shown in Figure 2.3. During periods of high particle flux one might observe so-called *geomagnetic storms*, where the magnetosphere is warped by the magnetic pressure [*Eastwood et al.*, 2015]. An illustration of the dominant zones of particle population is shown in Figure 2.4. Closest to the Earth, we find the plasmasphere which contains high-density, low-energy plasma. The inner, stable radiation belt is embedded in the plasmasphere. The outer radiation belt, dominated by high energy electrons (>10 keV) is highly variable in both position, energy and density. The plasmasheet is the source region for low energy auroral electron precipitation (<10 keV)

Electrons in the solar wind does not have energies allowing them to penetrate deep into the atmosphere, but trapped in the magnetosphere they are subject to different acceleration processes. Electrons from the plasma sheet (<10 keV) will reach down to ~100 km in the atmosphere. Electrons in the radiation belt, however, can be stored and further accelerated,

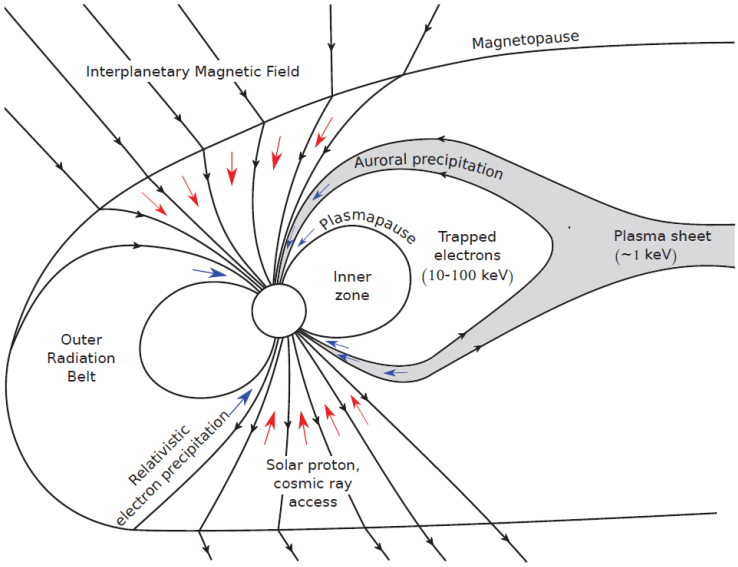

Figure 2.4: An illustration showing the dominant zones of particle precipitation. Adapted from *Thorne* [1980]

reaching relativistic energies allowing them to penetrate as deep as 50km. These particles transfer their energy to the atmosphere, ionizing particles and producing reactive hydrogen and nitrogen species which act as catalysts in destruction of ozone [*Thorne*, 1980]. Particles originating from the sun tend to be stopped in the middle and high atmosphere. Figure 2.5 illustrates penetration depths of different energetic particles as well as UV-radiation and x-rays. In this thesis we will refer to particles from SPEs, relativistic electrons and auroral electrons entering the atmosphere as *energetic particle precipitation*, or EPP. The impact from EPP on the climate is the main focus of this thesis.

2.1.4 Galactic Cosmic Rays

On a decadal scale, galactic cosmic rays seems to be anti-correlated with the solar wind flux, being stronger during solar minimum and weaker during solar maximum. These particles are generally very energetic, and could therefore in theory penetrate deeply into the atmosphere as illustrated in Figure 2.5. It's thought they could affect cloud generation, and thus have an effect on precipitation and the earth's albedo *Gray et al.* [2010], *Seppälä et al.* [2014]. We will not go into more details about this in this thesis.

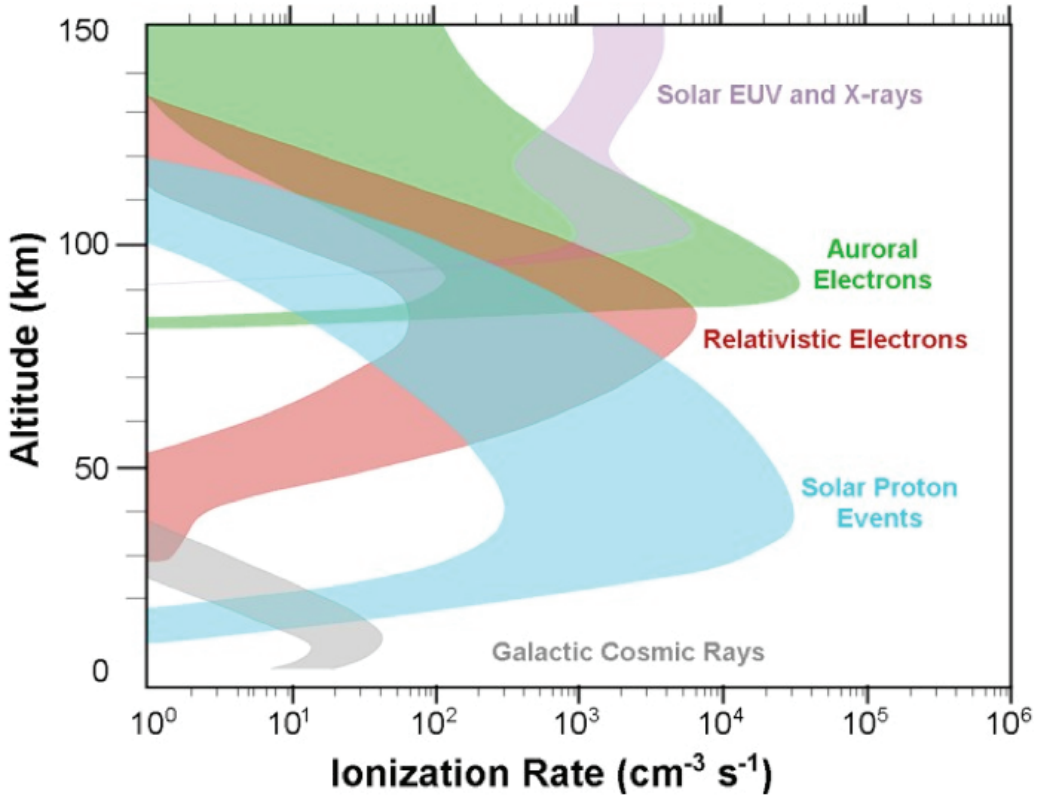

Figure 2.5: Figure showing penetration depths of different particle energies as well as solar UV and x-rays.

2.2 The atmosphere

The atmosphere is subject to influences from chemical, radiative and dynamical processes, such as ozone acting in chemical reactions as well as affecting the radiative budget, or atmospheric waves impacting the flow of wind in the atmosphere. Proper understanding of radiative balance, atmospheric chemistry and atmospheric dynamics is therefore important.

The atmosphere is often referred to as having layers sorted after their thermal properties, namely troposphere, stratosphere, mesosphere and thermosphere, with transition regions called tropopause, stratopause and mesopause respectively in between them, as illustrated in Figure 2.6. These atmospheric layers vary with latitude. The troposphere starts at

ground level and rises approximately 16 kilometers above ground over the equator, and approximately 8 km over ground over the polar regions. These differences are due to the stronger solar radiation the equator experiences compared to the poles. The troposphere is recognisable by decreasing temperatures by height up to the tropopause. In the stratosphere the temperature increases, mostly due to absorption from ozone, up to the stratopause at approximately 50 kilometers height. The mesosphere is found over the stratopause, where the temperatures again decreases with height, up to the mesopause, found between 85 and 100 kilometers depending on the season and latitude. These three layers have an approximately constant mixing ratio of 80% Nitrogen (N) and 20% Oxygen (O), and they are collectively referred to as the *homosphere*. The following layer of the atmosphere is the thermosphere, characterised by rapid temperature increases. It differs from the other layers, having a different chemical make-up where the relative abundance of the atmospheric species depends on diffusion separation between light and heavier compounds. It is referred to as the *heterosphere* [*Brasseur and Solomon*, 2005].

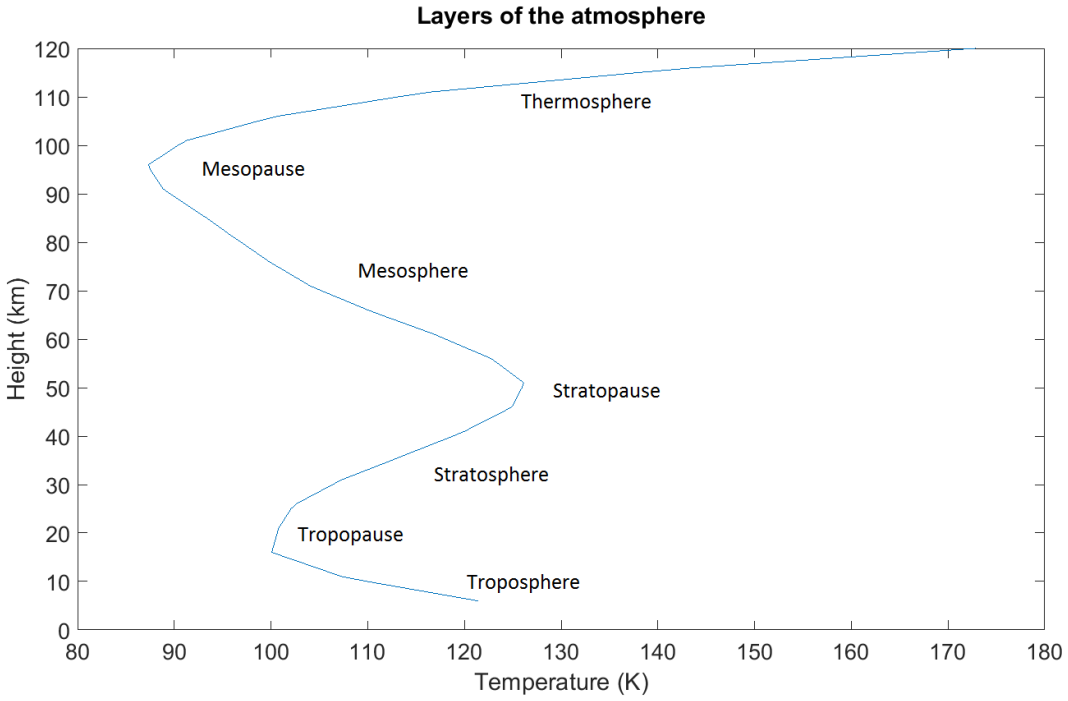

Figure 2.6: Vertical annual zonal mean temperature above 60°-80°N estimated from CIRA-86. The atmospheric layers with their respective pauses are illustrated.

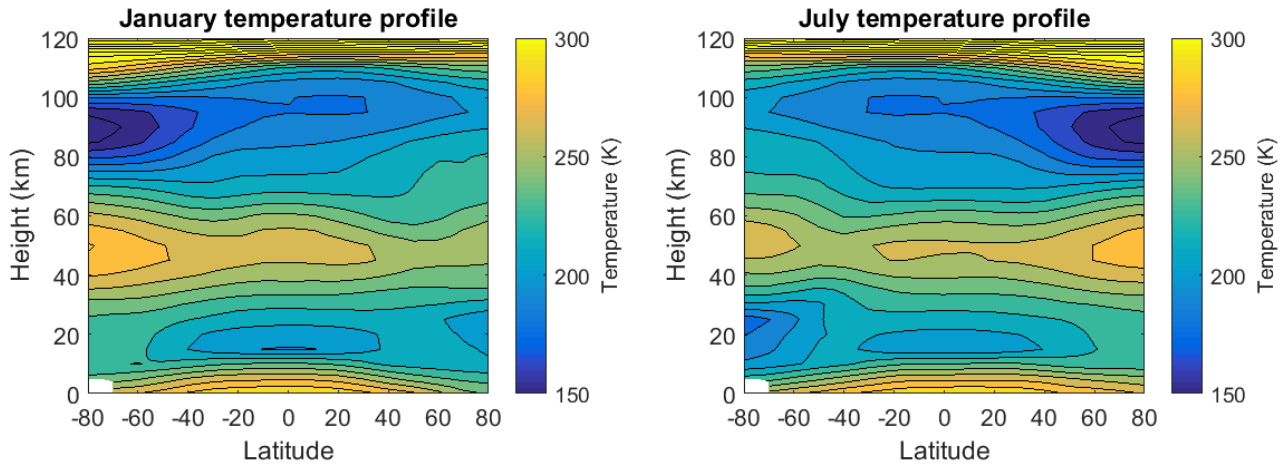

Figure 2.7: Latitude-height view of zonal mean temperatures, from CIRA-86, for the months January and July.

2.2.1 Radiative Balance

Figure 2.7 shows the temperature profiles of the atmosphere for January and July between 80° S-80° N. The month January represents northern hemispheric winter and southern hemispheric summer, and vice versa in the month of July. The summer hemisphere receives more electromagnetic heating from the sun, and experiences a positive radiative heating rate, with the opposite being true in the winter hemisphere. Based on the radiative balance the summer hemisphere should be hotter than its winter hemisphere counterpart. Figure 2.7, however, shows that the summer mesosphere is colder than the winter mesosphere, and the tropical tropopause is colder than both winter and summer tropopauses. This implies that dynamical processes are needed to fully explain the atmosphere [*Brasseur and Solomon*, 2005].

In the troposphere, at the equator and low-latitude summer hemisphere, air is transported upwards and towards the poles, sinking down at approximately 30° into the winter hemisphere, bringing heat to the winter hemisphere. This is known as the Hadley Cell, illustrated in Figure 2.8 [*Marshall and Plumb*, 2007].

In the stratosphere, the summer hemisphere ozone is heated by UV-radiation whilst the winter hemisphere experiences cooling from longwave radiation of ozone and carbon dioxide, setting up temperature gradients from the summer pole to the equator and winter

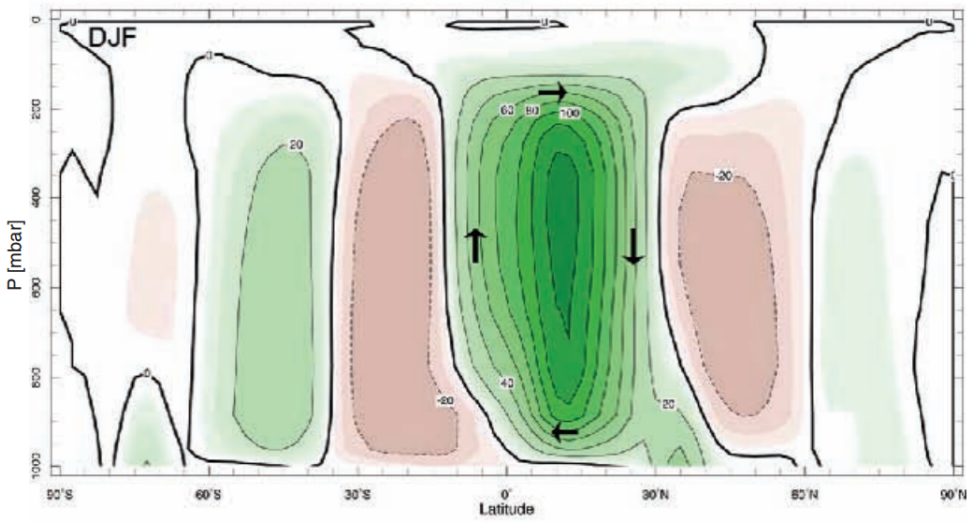

Figure 2.8: The mean meridional transport of air in the troposphere during December, January and February. Figure from *Marshall and Plumb* [2007].

pole. Atmospheric waves propagating from the troposphere to the stratosphere and mesosphere disturb the mean flow, allowing poleward transport at stratospheric altitudes and descending motions in the mid and high latitudes, causing adiabatic heating [*Haynes*, 2005]. This is referred to as the Brewer-Dobson circulation. In the lower stratosphere it goes from the tropics to the poles, whilst at higher altitudes it goes from the summer pole to the winter pole [*Smith*, 2012].

The mesosphere is mainly heated by UV-radiation via absorption by molecular oxygen and water vapour. The summer mesopause is noticeable because it holds a much lower temperature than its winter counterpart due to upward motion causing significant adiabatic cooling, while the opposite is true for the winter mesopause. This transport is driven by breaking of gravity waves [*Smith*, 2012].

Due to Earth's rotation, the coriolis force works against meridional transport [*Brasseur and Solomon*, 2005]. This means that the strongest winds in the atmosphere are mostly in the zonal direction. Winds are referred to as *westerlies* if they travel from the west to the east, and *easterlies* in the opposite case. Between 30°-40° latitude, and also at the so-called *polar vortex* the jets reach local maxima. These both act as particularily strong barriers against meridional transport of air [*Brasseur and Solomon*, 2005]. Figure 2.9 shows mean values of the wind taken in the zonal direction for January and July. The polar vortex is clearly

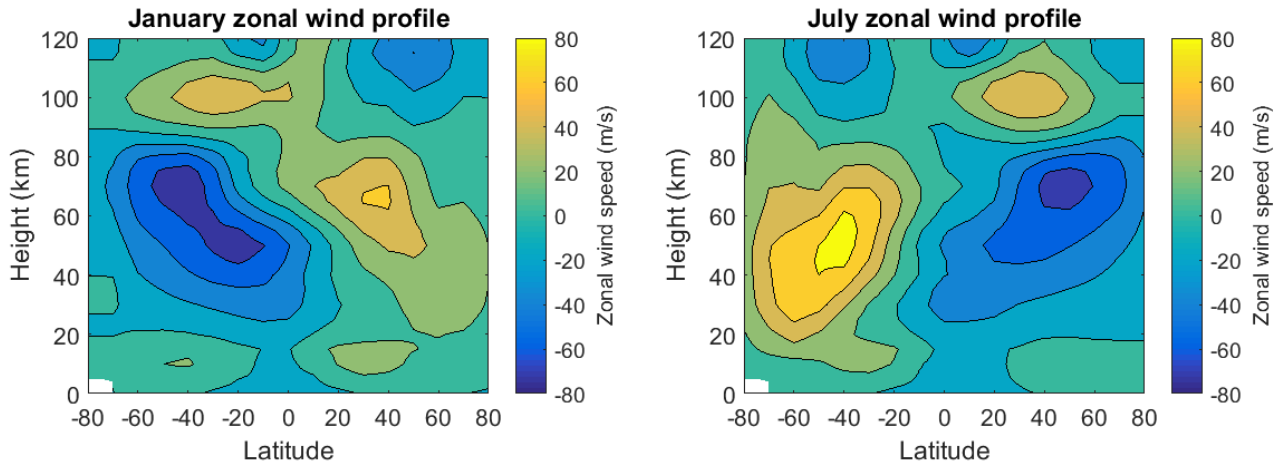

Figure 2.9: Similar to Figure 2.7, but for zonal mean zonal wind.

visible above 60° on the winter hemisphere.

2.2.2 Atmospheric waves

The waves are a key dynamic feature of the atmosphere. The atmospheric waves can be defined as propagating disturbances and differ depending on the restoring forces. These atmospheric waves often cause the wind variations regionally as well as globally. Generally the atmospheric waves are categorised into *gravity waves*, countered by buoyancy of the fluid, which opposes vertical displacements, and *inertial waves*, countered by the Coriolis force, which opposes horizontal displacements [*Brasseur and Solomon*, 2005].

Gravity waves typically arise from wind flowing above mountains, thunderstorms, jet stream shears and from solar radiation, and propagate upward into the atmosphere. Their amplitudes range from 10 to 1000 km, and their propagation in the atmosphere is dependent on wind motions, temperature, density, season and static stability. If the phase speed of the wave and the zonal wind speed are the same the wave is absorbed by the background flow. This means that upwards propagating waves are filtered by the background flow, as shown in Figure 2.10, causing gravity waves in the mesosphere to be mainly westward in winter and eastward in summer. If they are not absorbed, their amplitude grows so large that they produce strong vertical temperature gradient, causing the wave to become unstable and break. Depending on the wind and temperature, the

waves might not be absorbed, but rather reflected or refracted, travelling either horizontally or downwards *Murgatroyd* [1970].

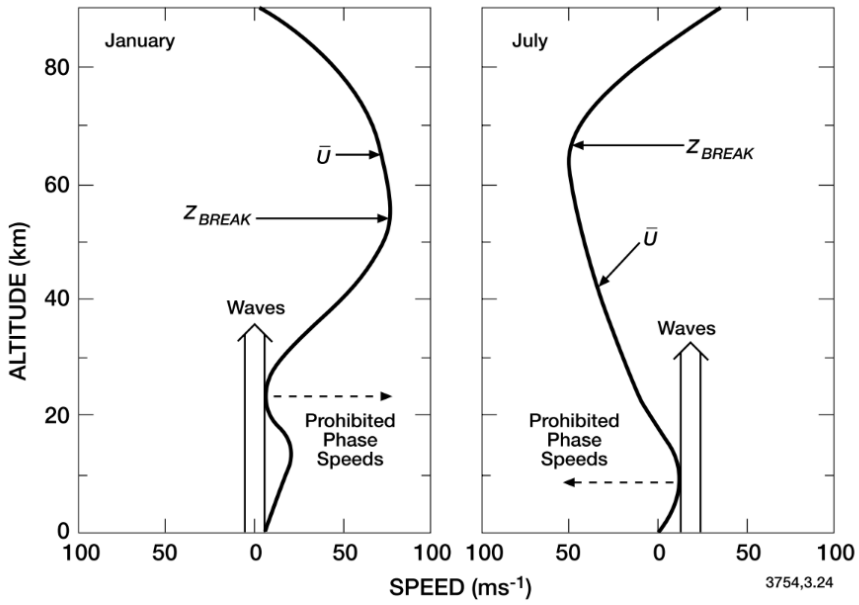

Figure 2.10: Approximate altitude profiles of the mean zonal winds in winter (left panel) and summer (right panel). The permitted phase speeds for the propagation of gravity waves and their breaking levels are also shown. Adapted from Lindzen(1981) [- find reference!]

Planetary-scale Rossby waves, also known as planetary waves, are inertial waves generally propagating westward of the mean flow. With large enough amplitudes, they might also propagate upwards into the stratosphere and mesosphere [*Brasseur and Solomon*, 2005]. They might occur due to flow over topography or latent heat release, and have timescales of days. Rossby waves impact the dynamics of the atmosphere, allowing for horizontal transport of heat. Due to wintert hemisphere stratospheric winds generally being westerlies, Rossby waves are more likely to propagate upwards during winter, making the winter stratosphere more disturbed than it's summer counterpart. The waves break in what's known as the surf zone, and may then disturb the polar vortex [*Haynes*, 2005].

2.2.3 The polar vortex

Above the polar regions from 16 kilometer altitude stretching into the stratosphere the polar vortex is found. The polar vortex is an area of low pressure surrounded by strong westerly winds known as the polar front jet stream. These westerlies trap cold air in the polar region, separating them from lower latitudes. Whilst the polar vortex is always present its strength is seasonal, being stronger in winter [*Rafferty*, 2014].

When the vortex is strong, it holds an almost circular shape. However when Rossby waves propagating into the stratosphere might disrupt the vortex, weakening the flow. These disturbances change the shape of the vortex, even detaching parts of it, as shown in Figure 2.11. This causes low pressure systems to move to lower latitudes, bringing cold air southwards and warm air northwards, known as a sudden stratospheric warming. Due to the lower wave activity in the southern hemisphere, the southern polar vortex is more stable than the northern [*Rafferty*, 2014].

2.2.4 Quasi-biennial Oscillation

In the tropical stratosphere the zonal winds show a peculiar behaviour with a periodicity of 2-3 years with alternating easterly and westerly wind regimes with downward phase propagation as shown in Figure 2.12. This is known as Quasi-Biennial Oscillation (QBO). This oscillation is mainly generated by wave-mean flow interaction [*Plumb*, 1977]. Planetary waves such as Rossby waves and K waves, tropically confined waves, and gravity waves are the main source for QBO. Although the QBO is confined to tropical stratosphere, its influence extends to different layers of the atmosphere, as well as different latitudes, such as modulating the strength of the polar vortex [*Baldwin et al.*, 2001].

Gray et al. [2010] reported that there is a connection between the phases of the QBO and the impact from geomagnetic activity upon the middle atmosphere. In the QBO easterly phase they observed an increase in geopotential height with solar activity, implying a heating below, and the opposite behaviour in QBO westerly years.

In an analysis by *Baldwin and Dunkerton* [2001], it was found that it was twice as likely to find a weak vortex during easterly QBO, and three times as likely to find a strong vortex

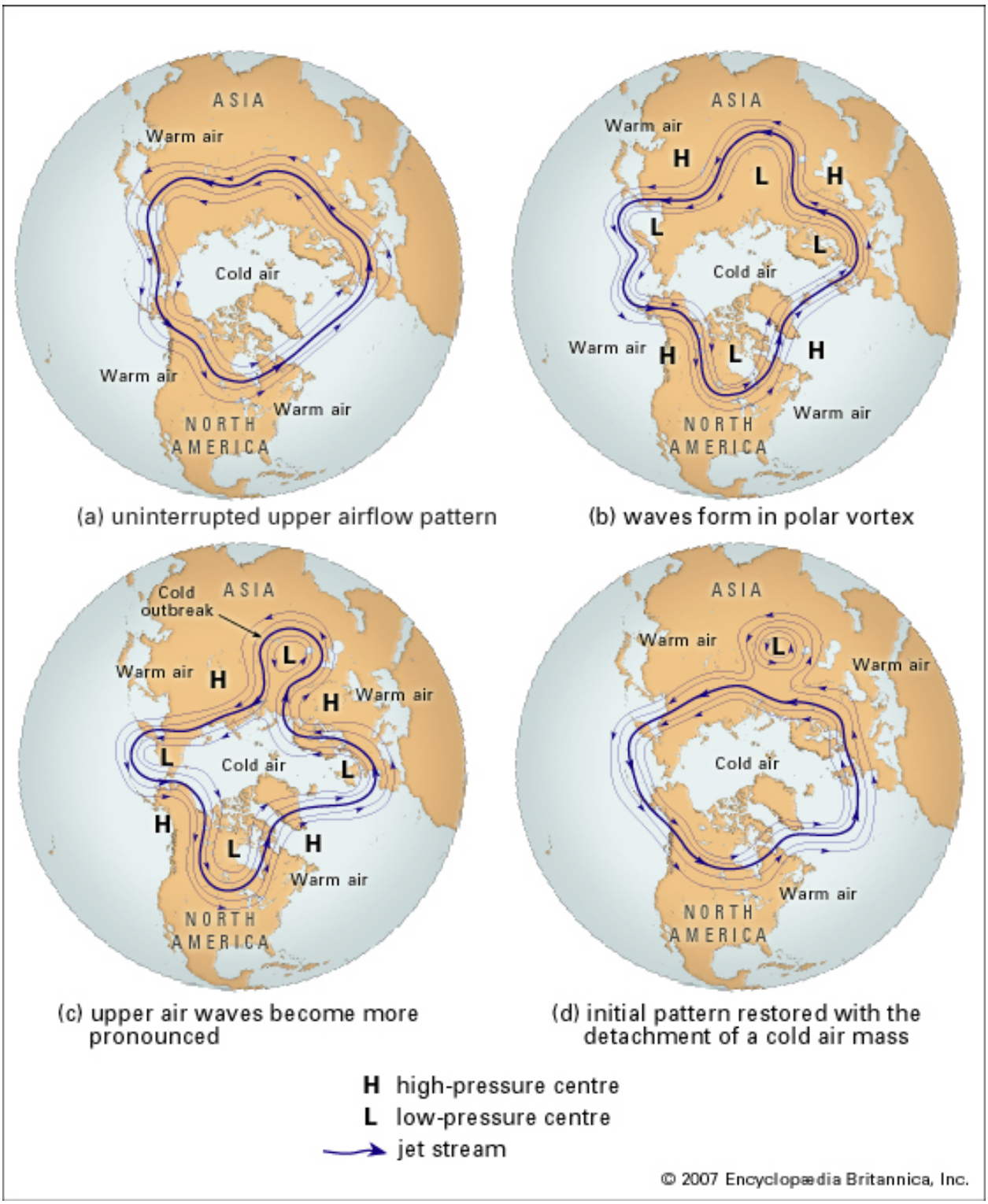

Figure 2.11: An illustration of how Rossby waves disturb the polar vortex, bringing low pressure systems to lower latitudes. From *Rafferty* [2014].

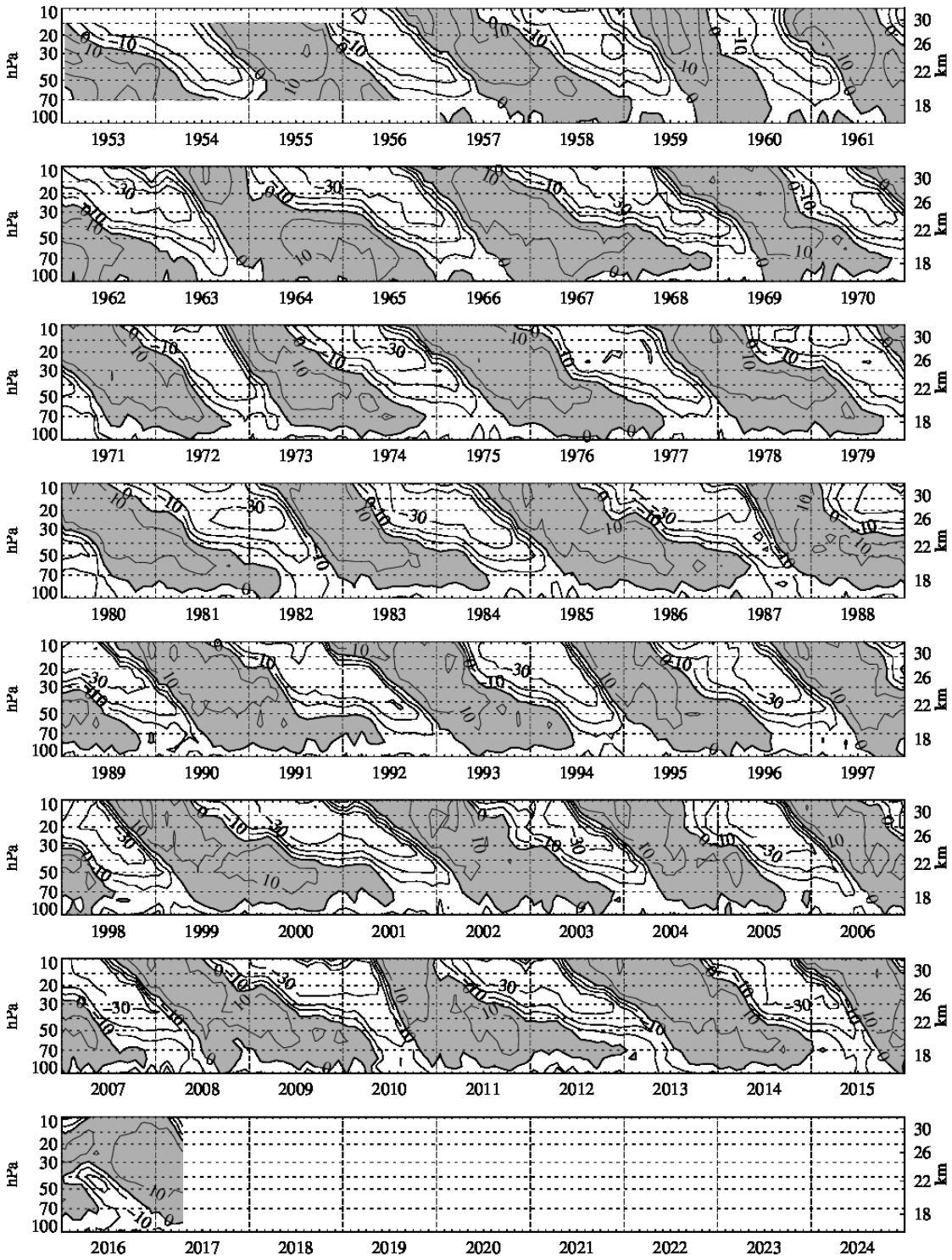

Figure 2.12: Time-height section of monthly mean zonal winds (m/s) at equatorial stations at Canton Island, Maldive Islands and Singapore. Figure from *Freie Universität Berlin*.

during westerly QBO, implying the phases of the QBO are important for modulating the polar vortex. A total breakdown of the polar vortex, a strong *sudden stratospheric warming*, is evident during the weak vortices of the easterly QBO. This modulation of the polar vortex by the QBO is explained through the holton-tan-effect [*Holton and Tan*, 1980, *Gray et al.*, 2010].

2.2.5 Sudden Stratospheric Warming

A sudden stratospheric warming is characterised by temperature spikes in the lower stratosphere, accompanied by lowered temperatures in the higher stratosphere and lower mesosphere. High wave activity decreases the background flow, which has a feedback to the planetary wave propagation which further decelerating the mean flow and pushing the polar vortex away from the poles. We observe a simultaneus meridional circulation, bringing heat from lower latitudes to the polar regions [*Brasseur and Solomon*, 2005]. During an SSW, temperatures may increase by more than 50 K, and during extreme events, so called *major warmings*, we might even see a reversal of the wind jets. The large events are rare, but smaller events can happen several times over a season. The last warming is generally seen in March or April, but in the case of large events it might already occur during January or February [*NASA Ozone Watch*].

Figure 2.13 shows an example of a SSW splitting the polar vortex in two. Note that the SSW affects ozone levels as well as temperatures. This type of event, with the split into two vortices, is called a wave-2 pattern. We might also see wave-1 pattern, where the vortex is simply "pushed off" the pole, creating one warm and one cold part on the northern hemisphere [*NASA Ozone Watch*].

2.2.6 Other atmospheric phenomena

Included in this section is information about some atmospheric phenomena possibly impacting solar effects that are not studied in detail in this thesis.

The El Niño and the Southern Oscillation (ENSO) are periodic fluctuations of Pacific Ocean surface temperatures and air pressure above, respectively. The two are closely connected.

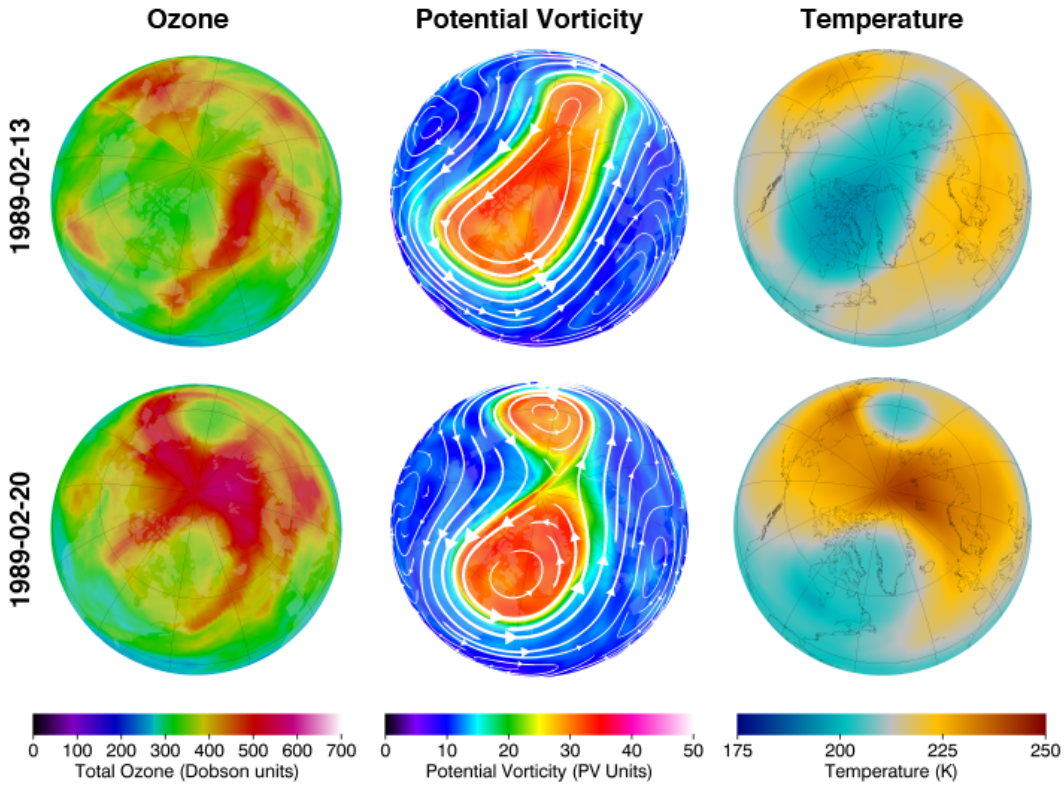

Figure 2.13: An example of a sudden stratospheric warming. Top Figures are a stable vortex before the warming, bottom are the disturbed vortex after the warming. Left shows total ozone column, middle shows potential vorticity (showing the location of the vortex), and right shows temperatures. Figure from *NASA Ozone Watch*.

The Southern Oscillation index is quantified by pressure differences at Darwin, Australia and Tahiti whilst the Oceanic Niño index is defined by sea surface temperatures in four regions of the Pacific Ocean *NOAA National Centers for Environmental Information* [b]. ENSO is well known to have an impact at higher latitudes, such as a weakening the polar vortex via enhancing planetary wave fluxes, increasing the rate of SSWs [*Butler et al.*, 2014].

Examples of other long term oscillations are the annual oscillation and the semi-annual oscillation. The annual oscillation is prominent at high latitudes, with larger amplitudes in the mesosphere than in the stratosphere. The stratospheric annual oscillation is caused by solar heating, while the mesospheric annual oscillation is associated with filtering of gravity waves. The Semi-Annual Oscillation (SAO) is a dynamic feature in the equatorial

stratopause of strong westerly winds at the equinoxes and strong easterly winds at the solstices. The SAO is caused by wave activity and advection from the summer hemisphere to the winter hemisphere. A similar phenomenon is visible near the mesopause, probably caused by gravity wave breaking [*Brasseur and Solomon*, 2005]. Though a tropical phenomenon, its effects are visible as far north as Tromsø in Norway [*Schwerdtfeger and Prohash*, 1956].

2.3 Solar Effects on the Atmosphere

The influence of solar irradiance variability, in particular the UV-variability, as well as the influence by the EPP is considered important factors for the natural climate forcing [*Seppälä and Clilverd*, 2014]. In this section, we summarize the pathway of which the different solar forcing might influence the atmosphere and polar surface temperature.

2.3.1 Total Solar Irradiation

The direct energy impact from both TSI and UV-radiation is strongest near the equator. As shown in part 2 of Figure 2.2, UV-radiation is mainly absorbed in the stratosphere, whilst lower energy radiation directly impact the surface. The latter is further thought to feed back, causing changes upward in the atmosphere. *Gray et al.* [2010] refers to this as a *bottom-up* mechanism. *Seppälä et al.* [2014] refers to model experiments investigating the global effect of changes in TSI upon the sea surface temperature, finding them to be less than 0.1 K, but while the estimates for total global effect of TSI are low it seemingly has a local effect, strengthening trade winds and intensifying rainfall in convergence zones. Increases in TSI lead to increased absorption at sea surface, increasing the sea surface temperature. Areas without high cloud cover are more sensitive to this, due to lower albedo. The extra heat causes extra evaporation and the excess moisture is moved with the trade winds towards so-called *precipitation zones*, areas with heavy rainfall. This is illustrated in Figure 2.14. These areas already have higher cloud cover, strengthened by this effect, meaning lower absorption and therefore less evaporation there, giving positive feedback to this effect [*Gray et al.*, 2010].

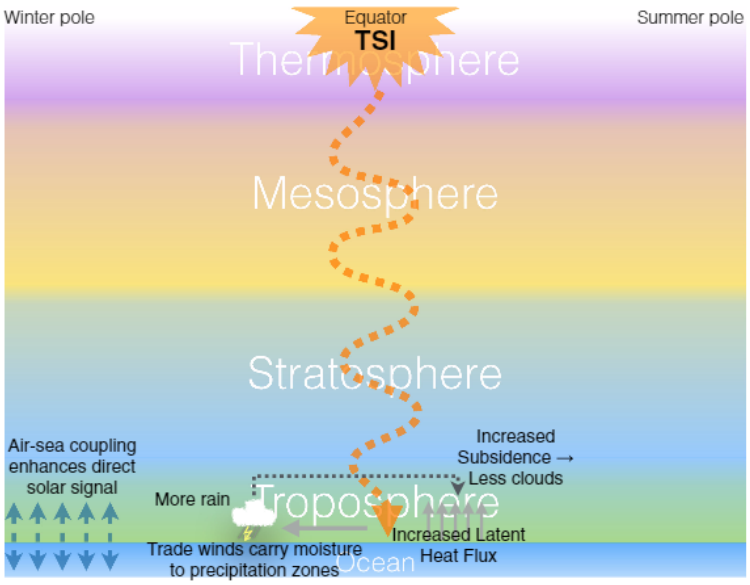

Figure 2.14: Increases in TSI affect locally, increasing evaporation near equator and increasing precipitation over precipitation zones. Figure from *Seppälä et al.* [2014].

2.3.2 UV-irradiance

Part 2 of Figure 2.2 shows, as mentioned, that most UV-radiation is absorbed by ozone in the equatorial stratosphere. Impacting in the stratosphere, it modulates local radiative heating at tropical latitudes, increasing the temperature and also stimulating the production of ozone, strengthening the effect. This heating changes the temperature gradient from equator to the poles, which again affects zonal winds. Changes in the zonal winds affect the propagation of planetary waves and how they interact with the mean flow, changing the filtering of the waves. As the effect progresses, a feedback is observed where the increased filtering changes the mean flow, thus changing the filtering again and strengthening the effect. This is referred to by *Gray et al.* [2010] as a *top-down* effect. These changes are seen as changes to the NAM-, AO- and NAO-indices, possibly on a 3 to 4 year time lag due to heat storage in the Atlantic Ocean, affecting sea surface temperature and pressure [*Seppälä et al.*, 2014].

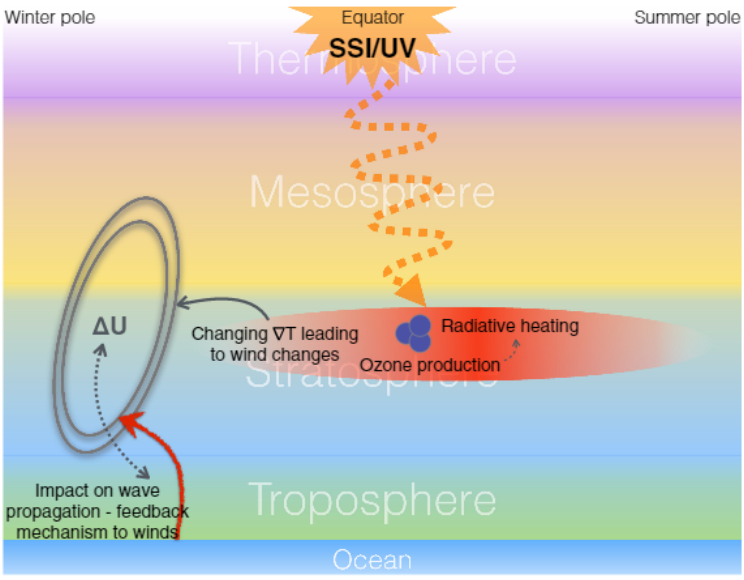

Figure 2.15: An increase in UV-radiation means an increase in absorption by and subsequentially temperature of ozone in the stratosphere. This changes the temperature gradient from equator to the poles, causing changes in the zonal wind and impacting wave propagation. Figure from *Seppälä et al.* [2014].

2.3.3 Energetic Particle Precipitation

The EPP, following magnetic field lines, generally occur at high latitudes. They enter the atmosphere, as far down as to the upper stratosphere for solar proton events and relativistic eletrons, creating chemical species such as HO_x and NO_x. The HO_x-species are short-lived and generally impact locally. NO_x has a lifetime of ~1 day under sunlit conditions, but in the dark winter polar atmosphere without photolysis EPP-produced NO_x can have an effective life span of months. In particular, the winter polar vortex constrains the NO_x to high latitudes where it can descend from the lower thermosphere to the upper stratosphere due to background winds and waves. HO_x and NO_x gases reaching the stratosphere will reduce ozone through catalytic reactions, reducing ozone levels significantly [*Gray et al.*, 2010], with local losses as high as 40% to 60% [*Seppälä et al.*, 2014]. As ozone is linked to cooling by emission of longwave radiation in wintertime, a temperature increase is observed at the stratopause levels. The mean meridional circulation will decrease, inducing a cooling anomaly deeper into the stratosphere [*Baumgaertner et al.*, 2011]. *Rozanov et al.* [2005] ran model simulations comparing years of low energetic electron

precipitation to years with induced high precipitation, finding ozone depletion of up to 30% in the polar latitudes along with surface temperature increases of up to 2.5 K over Russia, Europe and the US. *Baumgaertner et al.* [2011] ran models which found that increases in EPP led to positive tendencies in the NAM-index, associated with sea level heating over northern Eurasia and cooling over the eastern North Atlantic. *Lu et al.* [2008], using solar wind dynamic pressure as a proxy for particle precipitation, also found a positive effect upon the NAM index by the combined effects of EPP and high UV-irradiance, indicating strengthened polar vortex and weakened Brewer-Dobson circulation.

[*Seppälä et al.*, 2013] divided years into four groups by their geomagnetic activity and the total irradiance in an attempt to remove any potential effects from the UV-radiation from the results, finding reductions of upwards wave propagation, leading to a descending warming signal from the stratosphere to the troposphere. The signatures were found to be strongest with the combined impact from both UV and EPP. Stable winds or a strong polar vortex was found to be key in the descent of the NO_x towards the stratosphere, making the effect possible. *Seppälä et al.* [2009] finds stronger surface signature from geomagnetic activity when SSW-years are omitted from the study. It is argued that this is due to a more stable atmosphere allowing effects of geomagnetic activity to take place more efficiently.

The timing of this effect is not well established. Looking at Figure 2.5, we see that high energy particles such as from SPEs penetrate deep into the atmosphere and can impact more directly, whilst the lower energy electrons producing NO_x depend on the vertical background wind to have an impact.

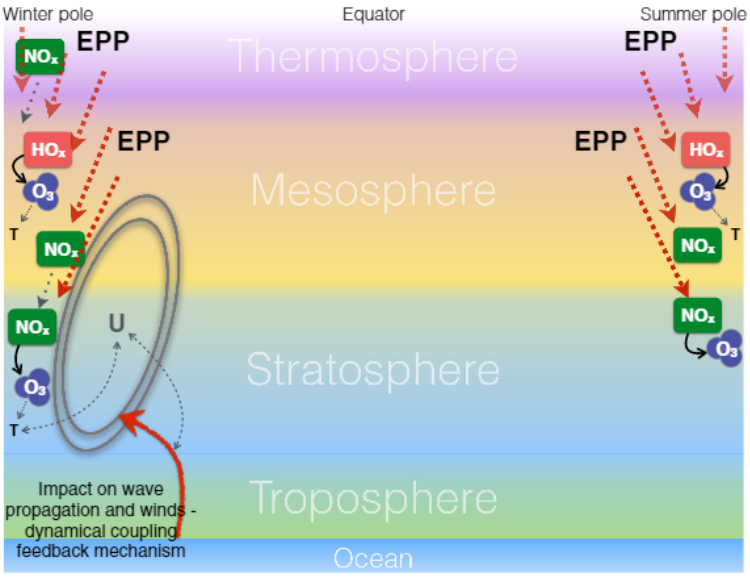

Figure 2.16: Energetic particle precipitation create HO_x and NO_x in the middle to upper atmosphere. If atmospheric conditions are good, these travel down to the stratosphere, dissociating ozone there, affecting the thermal balance. This causes a change in the temperature gradient from equator to the poles, impacting the zonal wind and thus the wave propagation. Note that in the summer hemisphere, the HO_x and NO_x are not long-lived enough to impact ozone, making this a seasonal effect. Figure from *Seppälä et al.* [2014].

3 Data and methods

In this section the data used to define geomagnetic activity and polar surface temperatures are explained. As little data of precipitating particle fluxes are available, the Ap-index is considered a decent proxy. To make simple calculations and correlations, the AO-index was considered a proxy of surface temperature, and MERRA-2 reanalysis data was used to determine the strength and geographic location of the geomagnetic impact upon the atmosphere. The methods used are explained, and the years of SSW, QBO phases and volcanic activity are defined.

3.1 The Ap-index

In this thesis we use the monthly averaged Ap to separate months into high and low fluxes of particle precipitation, as done in *Seppälä et al.* [2009]. The monthly averages are based on the 3-hour ap-index, which again are based on the quasi-logarithmic Kp-index. 13 magnetometers, 11 on the Northern Hemisphere and 2 on the Southern Hemisphere, measuring magnetic disturbances in the ionospheric electrojets, field-aligned currents, the ring current, the magnetopause current, and cross-tail current (all shown in Figure 3.1), are the basis for the Kp-index. An enhanced Ap-index thus imply intensification of currents in the ionosphere and magnetosphere, and high Ap-values gives a higher probability of particle precipitation. It does not, however, give us information about the particle fluxes, the altitude or the geographical distribution of the deposited energy. Using monthly averages does not provide information of the variability within the interval - heightened Ap-values stemming from a series of moderate storms and large, isolated storms are considered equal. We also do not consider if the storms occur in the start or towards the end of the period being averaged.

Maliniemi et al. [2013] investigated the correlation of seasonal (3-month averages) Ap with electron fluxes. Using NOAA/POES satellite measurements of precipitating electrons with energy ranges 30-100 keV and 100-300 keV in the years 1980-2015, they saw the solar cycle signature in the EPP. The years 1985, 1995 and 2004 were the maximum peaks, and they were lagged approximately 5 years to the solar cycle, happening in the declining phase. They found the Ap-index to be generally indicative of the EPP, but noted that considerable

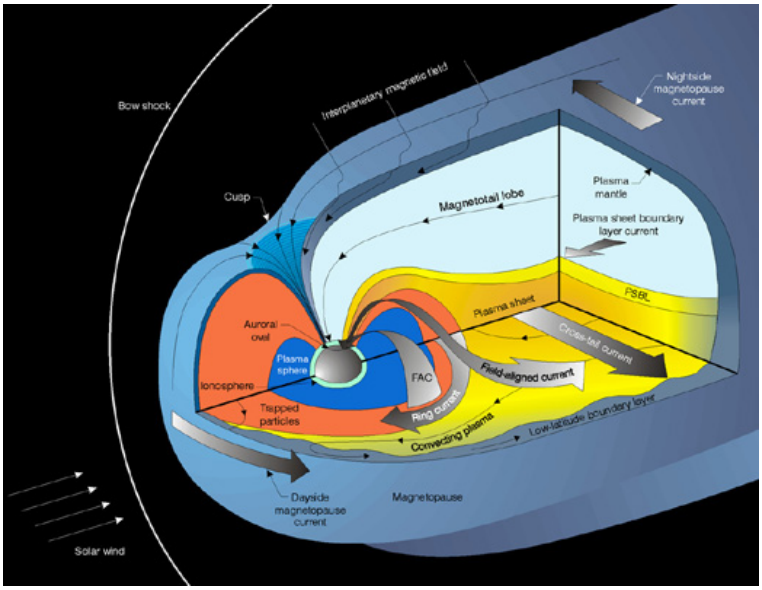

Figure 3.1: Figure showing currents in the magnetosphere. Figure from [*Southwest Research Institute*].

differences do exist especially for high energy electrons. See Figure 3.2.

The Ap of December, January and February is shown in Figure 3.3, as well as their median values, 55th percentile and 45th percentile. These percentiles are used to define high and low geomagnetic activity, respectively. This ensures a buffer between the group, as well as ensures enough years to make a statistical analysis possible.

3.2 The Arctic Oscillation-index

The Arctic Oscillation (AO), also known as the Northern Hemisphere Annular Mode (NAM), is a climate pattern found at approximately 55°N. In its positive phase, strong winds circulate the north pole and isolates the cold wind to high latitudes giving a strong polar vortex, whilst the negative phase has a weaker and distorted wave pattern, allowing cold arctic wind passage to lower latitudes as illustrated in Figure 3.4. The AO is, amongst others, linked to the distribution of sea ice in the arctic, and the distribution of ozone in the lower stratosphere [*Thompson*]. The AO is driven through a positive feedback between waves and the mean flow, and its effects may be visible in the stratosphere as well as the

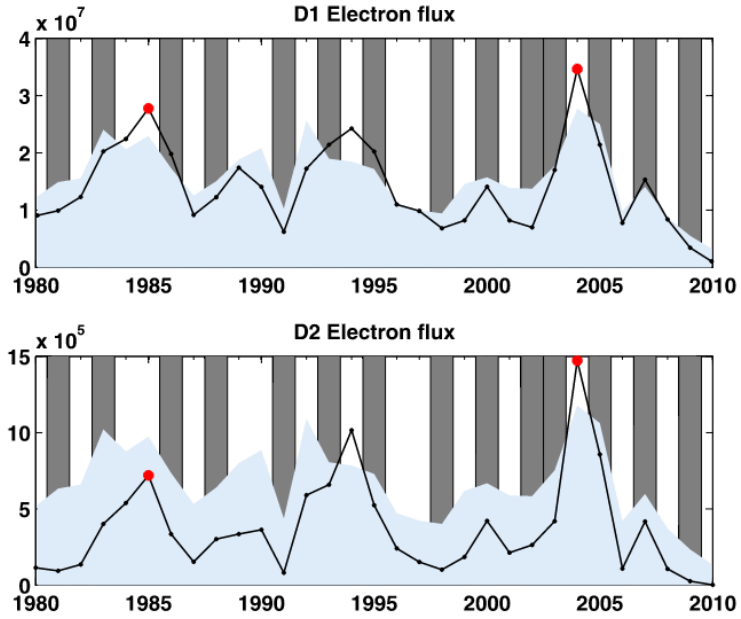

Figure 3.2: Correlation between Ap-index (blue) and EPP (black) at 30-100 keV (top) and 100-300 keV (bottom). Gray bars represent westerly QBO phase. Figure from *Maliniemi et al.* [2013]

troposphere. Positive trends in the AO described approximately half of the warming over Europe and Asia and 30% of the heating over the Northern Hemisphere as a whole. It also described approximately 40% of stratospheric cooling as well as 40 % of ozone depletion in March [*L'Heureux et al.*, 2010].

The AO-index is obtained by comparing daily anomalies in geopotential height of 1000 millibar between 20°-90°N to a monthly mean from 1979 to 2000 [*NOAA National Centers for Environmental Information*, c]. The AO-index is also highly correlated to the North Atlantic Oscillation (NAO) index, but gives information about the whole northern hemisphere instead of just the North Atlantic [*L'Heureux et al.*, 2010].

The names arctic oscillation, northern annular mode and north atlantic oscillation all refer to the same phenomenon of pressure differences on the northern hemisphere from polar regions to lower latitudes [*Thompson*], with NAO being Atlantic only and the other two being hemispheric, and as such the AO-index is highly correlated with the NAM-index. In this thesis we refer to the phenomenon as Arctic Oscillation and use the Arctic Oscillation index provided by *NOAA National Centers for Environmental Information* [c].

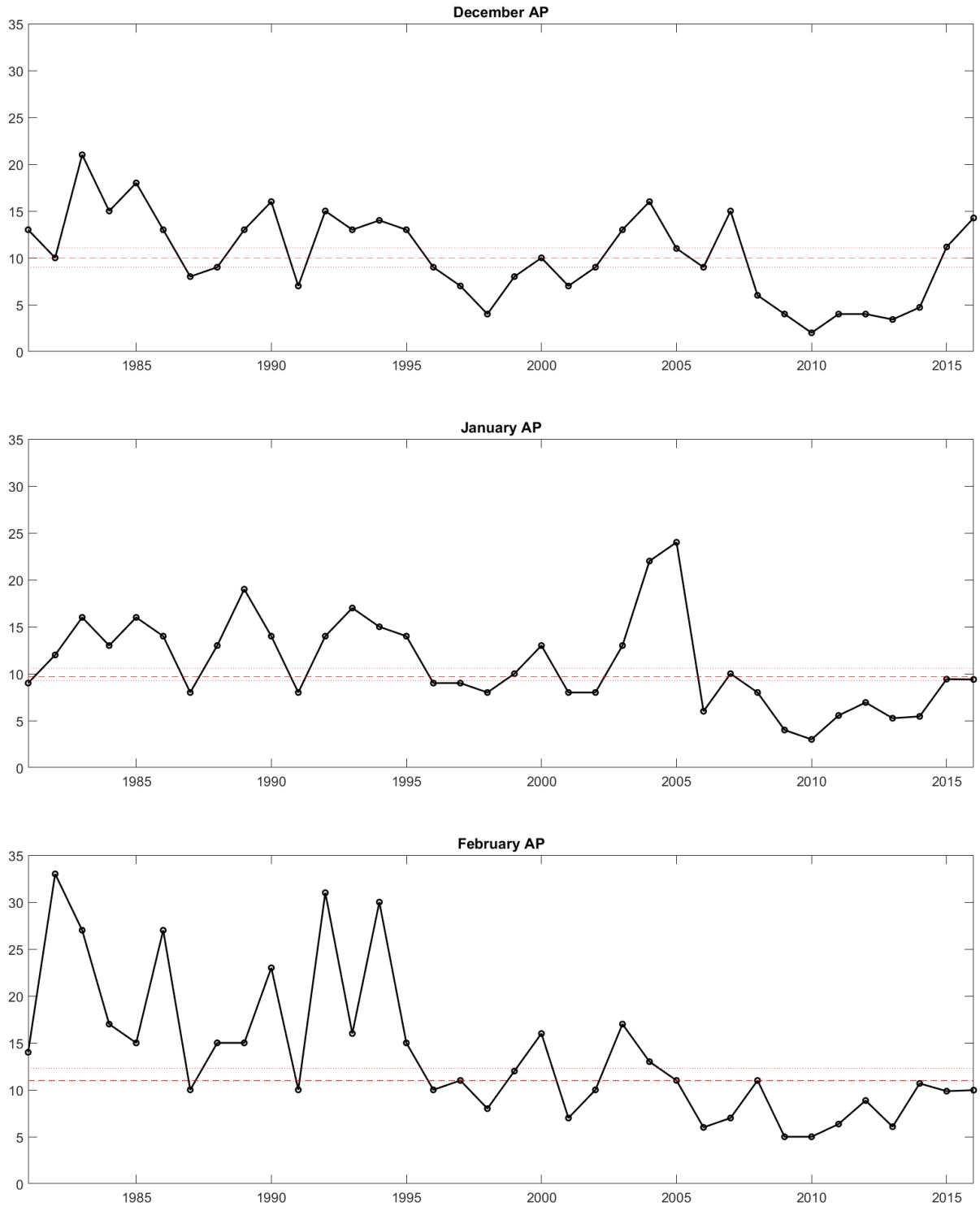

Figure 3.3: Ap-index of December (top), January (middle) and February (bottom), showing their median values as a dashed red line and the 55th and 45th percentiles shown as dotted red lines.

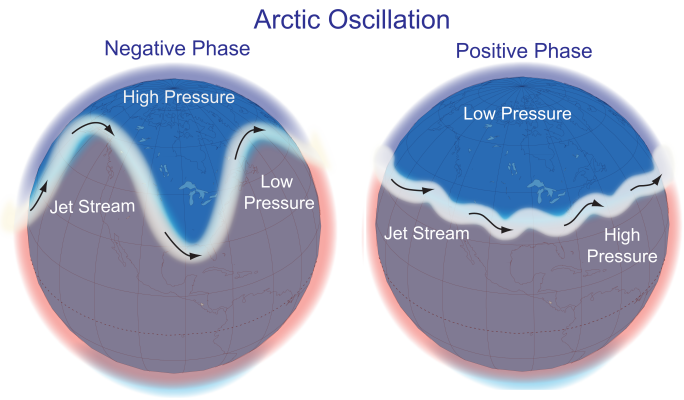

Figure 3.4: The phases of the Arctic Oscillation. Image from *Wikipedia* [a].

3.3 MERRA-2-reanalysis

An atmospheric reanalysis is produced by merging observations through a data assimilation procedure. They typically span over several decades and cover the entire surface of the Earth as well as the atmosphere, generally up to the middle atmosphere. Whilst a number of reanalyses exist (see Table B.1 in the appendix), in this thesis we will be using the Modern-Era Retrospective analysis for Research and Applications, version 2 (MERRA-2). MERRA-2 replaces the old MERRA reanalysis [*Rienecker et al.*, 2011], and covers the period from 1980 to present date. The MERRA-2 product named M2I6NVANA has been used, having a longitude and latitude grid of $0.625^\circ \times 0.5^\circ$, a time resolution of 6 hours and being analysed at 72 atmospheric levels from 985 hPa to 0.01 hPa, from surface to approximately 80 kilometers [*Global Modeling and Assimilation Office (GMAO)*, 2015]. The high altitudes reached in this reanalysis is the main reason for it being chosen, allowing signatures in the stratosphere and mesosphere to be studied. As MERRA-2 is a fairly new reanalysis, the data assimilation is very robust as it has access to more data. Monthly median values have been used to compensate for outliers in the data set. In this thesis, the winter months are studied, so the winter of 1981 is the first period studied, including November and December 1980.

Figure 3.5 shows fluctuations of the global annual mean temperature. The global mean temperature for the period 1980-2015 have been subtracted from each pressure level. The global temperatures in the lower stratosphere (100-10 hPa) show no obvious discontinuities

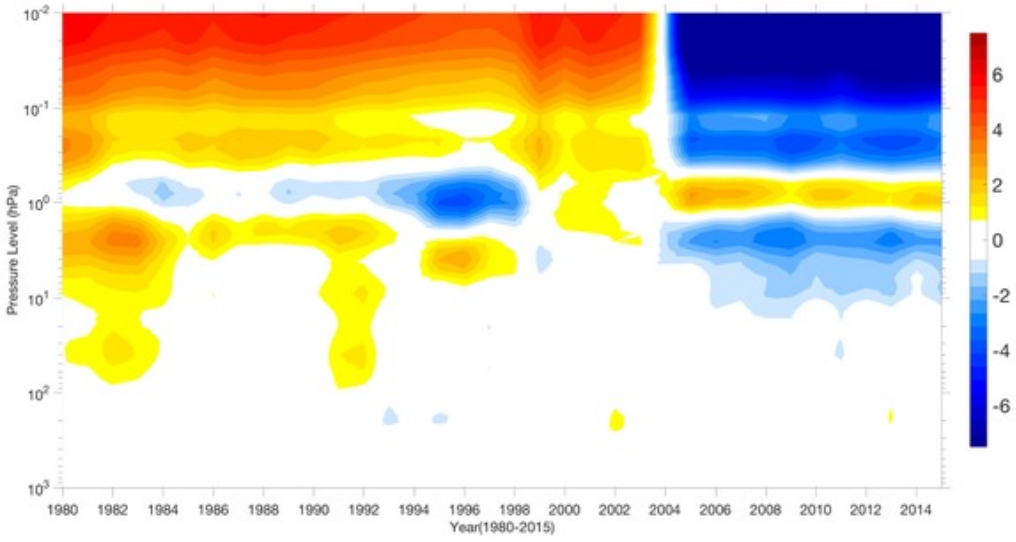

Figure 3.5: Variations of the global annual mean temperature.

as different instruments become availabe. Above 10 hPa, the scenario is different, and an anomaly is clearly visible, with lower temperatures after 2004 above 10 hPa, with an opposite anomaly around 1 hPa, indicating that data from these levels could impart a bias to our data. These anomalies might occur due to a change in data assimilation. We see two events where temperatures increase in the lower stratosphere as well, associated with large volcano eruptions at El Chichon in 1982 and Pinatubo in 1991. In order to check whether the deviations are due to latitudinal differences, we plotted the latitudinal variations of monthly zonal mean temperatures for the period 1980-2015 for the uppermost five pressure levels, shown in Figure 3.6. The figure shows a clear seasonal and latitudinal temperature variation. Interestingly, the temperature deviations after 2004 are evident at all latitudes. These deviations might occur due to changes in data assimilation [*Gelaro et al.*, 2016]. The large deviations at higher levels might influence the climatological estimations.

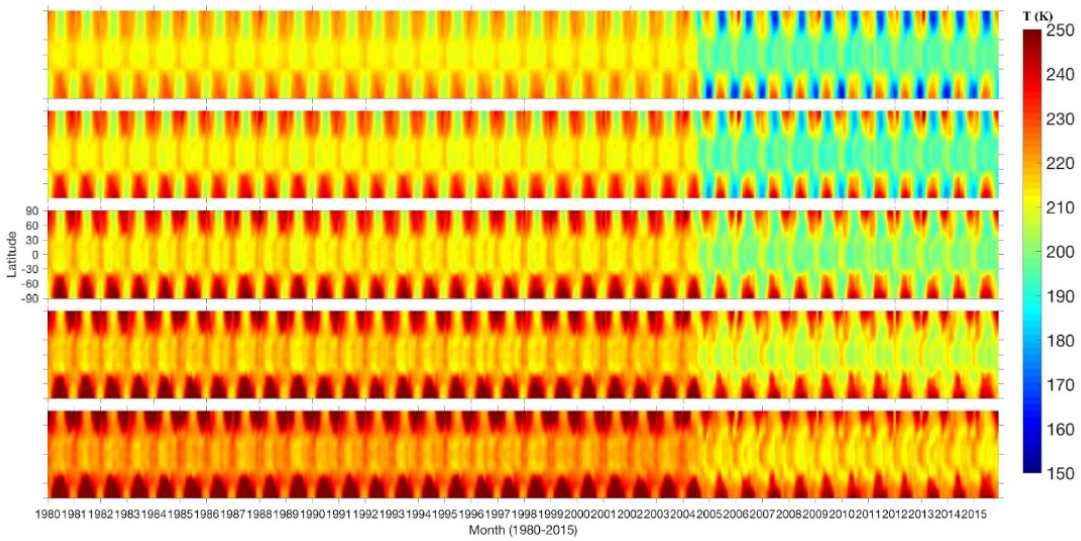

Figure 3.6: Month-latitude variation of zonal mean MERRA-2 temperatures for 5 model levels, from the top: 0.01 hPa, 0.02 hPa, 0.0327 hPa, 0.0476 hPa and 0.0660 hPa.

3.4 Defining the SSW, QBO and volcanic activity years

Charlton and Polvani [2007] defines major SSWs over the winter season by an algorithm depending on the daily mean zonal winds at 60°N and 10hPa. These events are listed at *NOAA Earth System Research Laboratory*. In this thesis we consider a year a SSW year if a major warming occurs in December, January or February, with December being included in the following year (e.g. December 1980 is considered winter 1981). Table 3.1 lists the years with sudden stratospheric warmings.

SSW years	1952, 1957, 1958, 1960, 1963, 1966, 1968, 1970, 1971, 1973, 1977, 1979, 1981, 1985, 1987, 1989, 1991, 1999, 2001, 2002, 2003, 2004, 2006, 2007, 2008, 2009, 2010, 2013

Table 3.1: The years with sudden stratospheric warmings.

The QBO phase years are defined in this thesis by the mean of their 50hPa December, January and February values, with December being included in the winter of the following year, as for the SSW years. Positive values give westerly QBO, negative values give easterly

QBO. The data is provided by *Freie Universität Berlin*, and the years are listed in table 3.2. As the QBO-years are only considered in the MERRA-2 reanalysis data, only the years after 1980 are shown.

Easterly QBO years	1980, 1982, 1984, 1985, 1987, 1990, 1992, 1997, 1999, 2001, 2002, 2004, 2006, 2008, 2010, 2013, 2015
Westerly QBO years	1981, 1983, 1986, 1988, 1989, 1991, 1993, 1994, 1995, 1996, 1998, 2000, 2003, 2005, 2007, 2009, 2011, 2012, 2014, 2016

Table 3.2: QBO phase years, based on 50 hPa equatorial zonal winds.

After 1980, the years of 1982 and 1991 are years of considerable volcanic activity, and the years directly following are excluded in some parts of the thesis. In these years El Chichón and Mount Pinatubo, respectively, had eruptions exceeding a Volcanic Explosivity Index of 5. See *Wikipedia* [b] for full list.

3.5 Methods

As a starting point, the Pearson correlation coefficients between the Ap-index and the AO-index for different time periods and seasons with and without sudden stratospheric warming years, along with their respective p-values. This was done as a precursor to define when the effect, if any, of geomagnetic activity has on the polar surface temperatures. The Pearson correlation coefficient was chosen because the effect is thought to be linear. High correlation does not imply a causal link, and as such the results found are only considered to be guidelines for further study.

The MERRA-2 reanalysis temperature data were separated into positive AO years, SSW years and years according to the phase of the QBO at four levels in the atmosphere: 1000 hPa (ground level), 850 hPa ($\approx$1.5 km), 10 hPa ($\approx$30 km) and 1 hPa ($\approx$50 km). This was done to see determine the characteristics of these phenomena with respect to the atmospheric temperatures. Stratosphere temperatures are of importance because ozone is an important driver for its thermal properties, and catalytic destruction of ozone is considered the main pathway EPP impacts the lower atmosphere. The AO climatology

was found from November to February whilst the SSW and QBO years were mean values over December, January and February. The AO was found over four months to see its evolution over the winter season and to easily compare with high activity years. The QBO and SSW are not studied in as much detail, and only seasonal averages are found for simplicity.

The MERRA-2 reanalysis temperature data were also divided into high geomagnetic activity and low geomagnetic activity, as defined earlier in this chapter. Temperature anomalies from high activity years were found compared to total climatology and low activity years by subtracting the annual means of the total climatology (in one case) and low activity years (in the other) from the high activity years at the same four levels as with the climatologies above. A students t-test was run to determine the significance of the results found. The student's t-test was chosen due to it being fairly robust with a low number of data points.

To avoid bias towards different atmospheric phenomena, the high and low activity years within the phases of the QBO and the SSW years were found and compared to each other. This was done to determine if the signatures observed were due to a bias in the selection to one or the other phenomenon, or in fact due to increased particle precipitation. The high activity years were also compared to the total climatologies to determine if the effects of EPP are changed in different atmospheric settings. Students t-tests were run to determine the significance of these results as well.

4 Results

This chapter presents the findings of the thesis. First, correlation between the Ap- and AO-indices were calculated for different time periods, seasons and lags. This is done to determine when during which period of the year the effect, if any, will take place, and to determine the time lag of the effect. The relationship was investigated in three different ways: Pearson correlation coefficients were found between monthly averages of the Ap- and AO-indices, Pearson correlation coefficients were found for monthly averages of the Ap-index compared to the wintertime monthly averages of AO to determine changes in lag over a season, and a Super Epoch Analysis was performed to determine lag. These cover the period 1950-2016 and the period 1980-2016.

Secondly, we investigated the climatological temperatures during different atmospheric states, such as positive AO, SSW years, easterly and westerly QBO as well as years impacted by volcanic activity. This enables us to see if a potential EPP signature is different from the climatological AO, as well as understand how a potential bias in our data towards a specific state will impact our results.

Finally, years were divided into high activity and low activity as defined in the Chapter 3.1. Temperature anomalies from high activity periods were compared to low activity years as well as total climatology, with and without time lag. Temperature anomalies are also investigated for high activity periods within different phases of the QBO and SSW years to determine how these atmospheric phenomena impact the effects of EPP.

4.1 Correlation of the Ap- and AO-indices

Figure 4.1 shows monthly variations Ap- and AO-indices from January 1950 to May 2016, years when data for both these indices are available, January 1980 to May 2016, years studied in detail in MERRA-2, and December, January and February starting in December 1950, ending in February 2016, months studied in detail. The cyclic nature of the Ap-index is visible. They do not at first glance seem to be strongly correlated. The winter months were shown because the effect of geomagnetic activity is supposedly confined to winter.

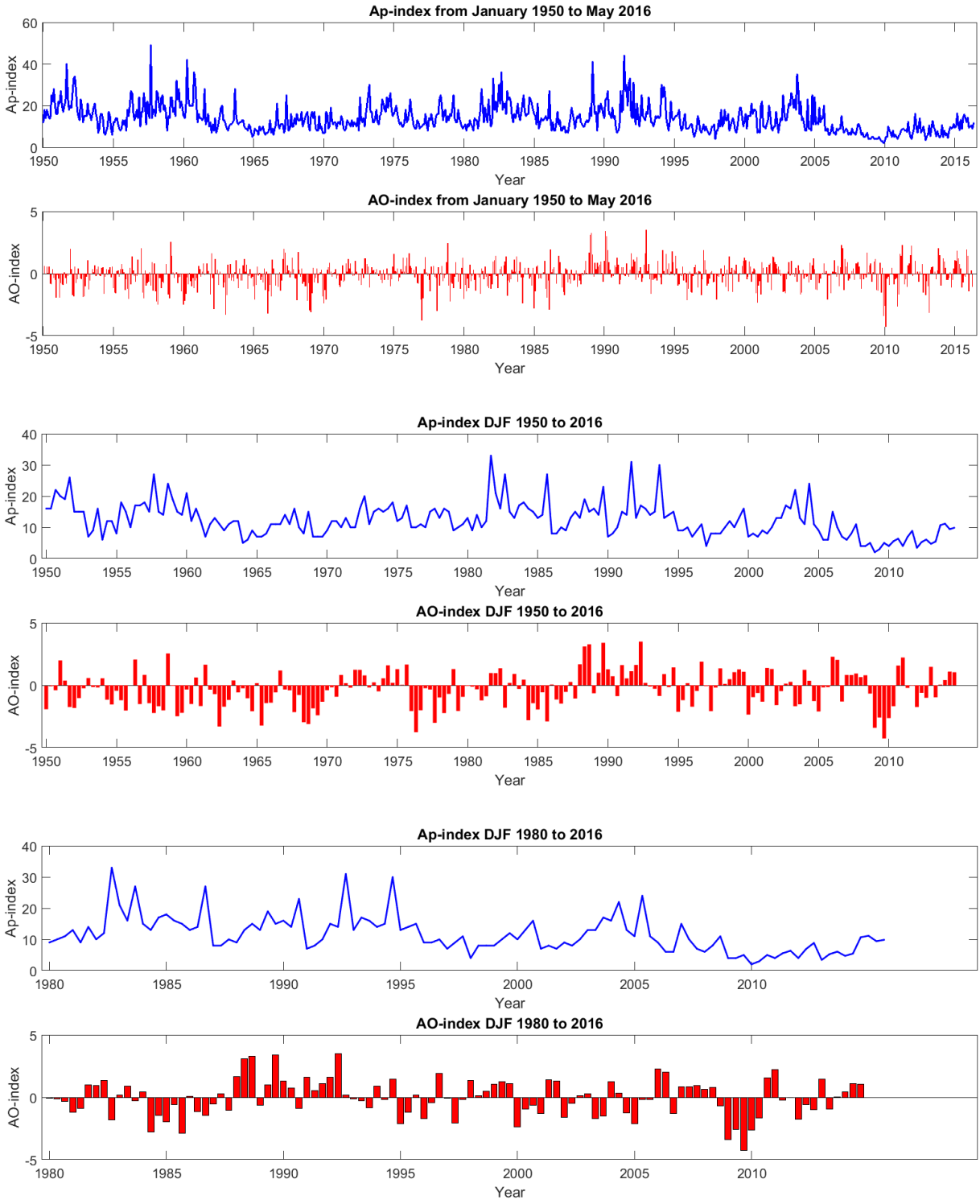

Figure 4.1: The Ap-index (blue) and AO-index (red) from January 1950-May 2016 (top), their December, January and February values starting in December 1950 and ending in February 2016 (middle), and the same for 1980-2016 (bottom).

Table 4.1 lists the Pearson correlation coefficients of the monthly mean values of the Ap- and AO-indices along with their respective p-values over different time periods . Looking at all months from 1950 to 2016, we see no significant (below 0.05 p-value) correlation, but focusing at the years 1980-2016 (see Table 4.2) we find a significant, but weak correlation between the monthly Ap- and AO-indices. Dividing 1950-2016 into winter and summer, we find no significant correlation between the two. Looking closer at seasonal values, however, we find a significant correlation of 0.25 during winter months (DJF).

Notes	Data sets	Correlation	p-value
All months, no time lag	1950-2016	0.04	0.26
Specific months, no time lag	Wintertime (Oct-Mar)	0.19	0.14
	Summertime (Apr-Sep)	-0.10	0.43
	Dec-Feb	0.25	0.04
	Mar-May	-0.12	0.33
	Jun-Aug	0.00	0.99
	Sep-Nov	-0.20	0.11
1 month lag	Ap Nov-Jan, AO Dec-Feb	0.22	0.08
	Ap Dec-Feb, AO Jan-Mar	0.21	0.08
2 months lag	Ap Nov-Jan, AO Jan-Mar	0.11	0.36
	Ap Oct-Dec, AO Dec-Feb	0.13	0.28
4 months Ap, 3 months AO, 2 months lag	Ap Oct-Jan, AO Dec-Feb	0.19	0.12
SSW years removed	All months, no time lag	0.03	0.47
	Dec-Jan	0.19	0.24
	Ap Nov-Jan, AO Dec-Feb	0.25	0.13

Table 4.1: Correlation between Ap and AO over different time periods and with different time lags. All the periods are from start of January 1950 to end of May 2016.

Seppälä et al. [2009] reported finding the highest correlation between sea surface temperatures and geomagnetic activity if one took mean values of Ap from October to January, and looked at the surface signature for three months starting with a two months delay. In order to determine a potential time lag of the effect, we calculated the Pearson correlation coefficients for 1 month and 2 months lags, as well as the the time lag suggested by Seppälä. For a 1-month lag we find the highest correlation of 0.22 with Ap-index over November to January and AO-index from December to February. A similar value of 0.21 was found with Ap from December to February and AO from January to March. Mind that this is

not significant at the 5% level, but it is at the 10% level. For two month lags we find no significant correlation even at the 10% level. Calculating correlations for Ap from October to January and AO from December to February, following *Seppälä et al.* [2009], revealed no significant correlation. Note that the Seppälä paper used sea surface temperature whilst we use indices, so our results are not perfectly analogue to those found there.

Seppälä et al. [2009] found more significant results when SSW-years were omitted. After excluding 28 years of data (years shown in table 3.1) where a sudden stratospheric warming occured, we found the correlation coefficients for all months, December-February and Ap from November to January with 1 month time lag, as listed in Table 4.1. None of these showed any significant correlation in contrast to the Seppälä paper.

Table 4.1 shows that the period from 1980 to 2016 is significantly correlated with the AO over the same period. This is also the period studied in detail in this thesis with the MERRA-2 reanalysis, so a closer look was in order. Table 4.2 shows similar results to table 4.1, but for the period 1980-2016. Surprisingly, the mean Ap-index values of the months April to September of those years are significantly correlated to the corresponding AO-index with a correlation of 0.37, higher than any of the previous results and possibly explaining the all-year correlation from earlier. This is however not visible as significant correlation in any of the summer months, nor in spring or autumn. As potential EPP effects during summertime falls outside the scope of this thesis, we will not try to explain this further. An illustration of the Ap- and AO-indices over this time is found at Figure B.1 in the Appendix.

The other correlations are similar to those covering the period 1950-2016, but less significant, with no results significant at the 5% level. The correlation of the Ap-index and AO-index as mean values over December, January and February are significant at the 10% level (r = 0.29) , as is the one month lag with Ap-index taken as mean values from December to February and the AO-index taken as mean values from January to March (r=0.32). This means that the correlation of one month lag is higher in the period 1980-2016 compared to 1950-2016.

In a further attempt to reveal a potential lagged dependance, the correlation coefficients for the Ap-index over the three winter months separately compared to the AO-index over six months were investigated. These are shown in table 4.3 with all years and table 4.4 without

Notes	Data sets	Correlation	p-value
All months, no time lag	1980-2016	0.12	0.01
Specific months, no time lag	Wintertime (Oct-Mar)	0.28	0.11
	Summertime (Apr-Sep)	0.37	0.03
	Dec-Feb	0.29	0.09
	Mar-May	0.11	0.50
	Jun-Aug	0.20	0.23
	Sep-Nov	-0.05	0.79
1 month lag	Ap Nov-Jan, AO Dec-Feb	0.26	0.12
	Ap Dec-Feb, AO Jan-Mar	0.32	0.06
2 months lag	Ap Nov-Jan, AO Jan-Mar	0.19	0.26
	Ap Oct-Dec, AO Dec-Feb	0.19	0.27
4 months Ap, 3 months AO, 2 months lag	Ap Oct-Jan, AO Dec-Feb	0.23	0.18
SSW years removed	All months, no time lag	0.10	0.13
	Dec-Jan	0.20	0.41
	Ap Nov-Jan, AO Dec-Feb	0.32	0.18

Table 4.2: Similar to Table 4.1, but for 1980-2016

SSW years. It is also illustrated in Figure 4.2. November Ap has the highest correlation with December AO, however this is only significant at the 10% level. When SSW-years are removed, the highest correlation is in January, closely followed by December, but none of these are significant. December Ap has no significant correlations when you consider all years, but when SSW-years are removed, we find a strong significant correlation of 0.33 with the January AO. January Ap is significantly correlated with January and, interestingly, December AO, implying an effect back in time. Removing SSW-years, the December AO correlation disappears, and we see a strong, significant correlation with January AO.

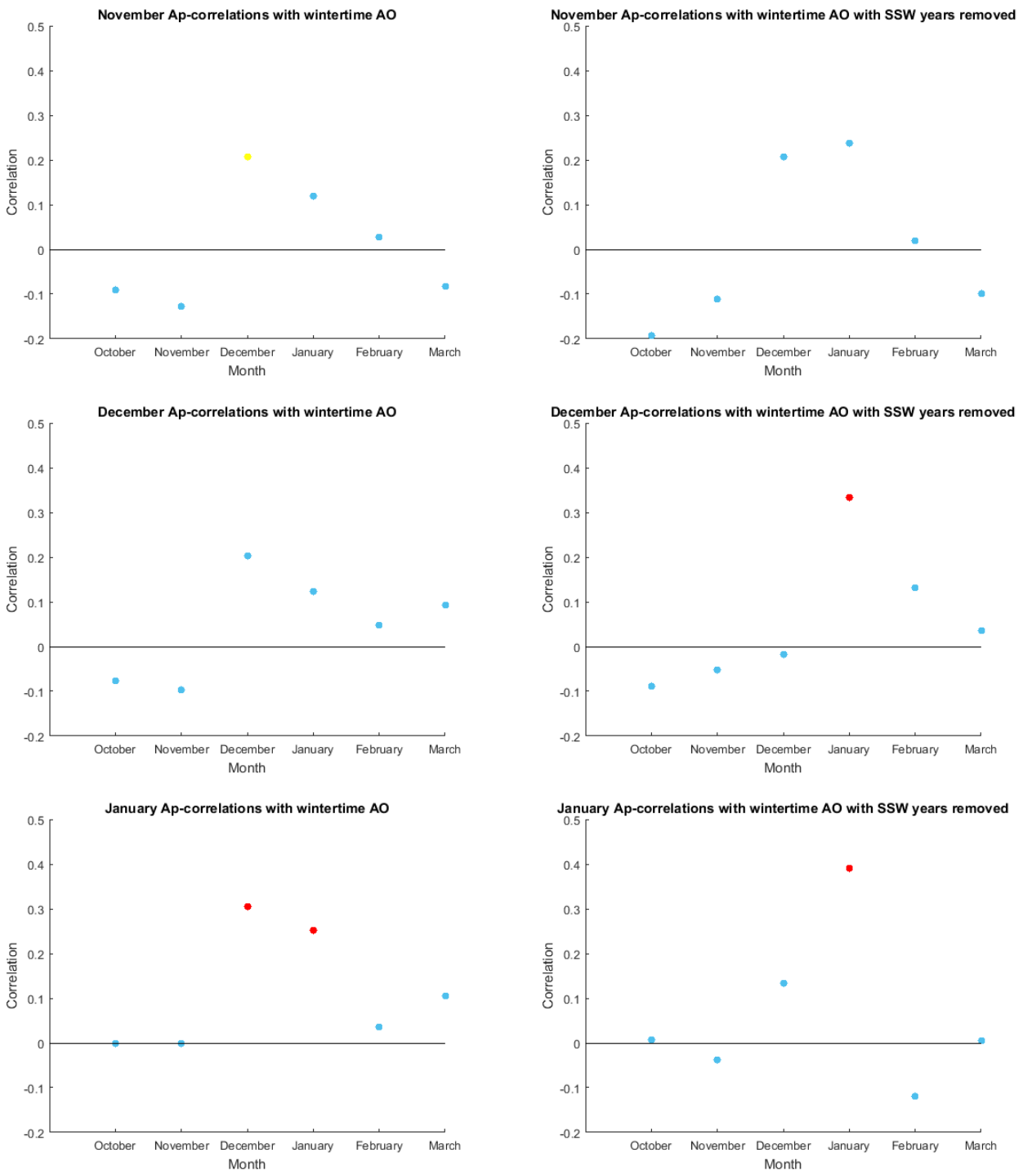

Figure 4.2: Correlation with different months of Ap over AO winter months. Black is 1% confidence interval, red is 5% confidence interval and yellow is 10% confidence interval. The left Figures are with SSW years included, whilst the right ones the SSW years have been removed.

November Ap	Correlation	P-value	December Ap	Correlation	P-value	January Ap	Correlation	P-value
October AO	-0.09	0.47	October AO	-0.08	0.54	October AO	0.00	0.99
November AO	-0.13	0.31	November AO	-0.10	0.44	November AO	0.00	1
December AO	0.21	0.09	December AO	0.20	0.10	December AO	0.31	0.01
January AO	0.12	0.34	January AO	0.12	0.32	January AO	0.25	0.04
February AO	0.03	0.82	February AO	0.05	0.71	February AO	0.04	0.78
March AO	-0.08	0.51	March AO	-0.09	0.46	March AO	0.11	0.40

Table 4.3: Correlation between specific months of Ap and wintertime AO

November Ap	Correlation	P-value	December Ap	Correlation	P-value	January Ap	Correlation	P-value
October AO	-0.19	0.25	October AO	-0.09	0.60	October AO	0.01	0.97
November AO	-0.11	0.50	November AO	-0.05	0.76	November AO	-0.04	0.82
December AO	0.21	0.21	December AO	-0.02	0.91	December AO	0.13	0.42
January AO	0.24	0.15	January AO	0.33	0.04	January AO	0.39	0.02
February AO	0.02	0.91	February AO	0.13	0.43	February AO	-0.12	0.48
March AO	-0.10	0.56	March AO	0.04	0.83	March AO	0.00	0.98

Table 4.4: Correlation between specific months of Ap and wintertime AO with SSW-years removed

A Super Epoch analysis is performed by comparing values before and after an event set by comparing criteria set to a randomised sample of the same data. In this thesis 800 iterations were used, selecting random periods of the AO-index to act as a reference. To avoid that the selected events are biased toward the declining phase of the solar cycle, the high activity events are defined as an Ap-index value larger than 5 nT than the yearly average, resulting in 6 events.In case several events happen over the same season, only the first event is considered. Figure 4.3 illustrates the wintertime AO-index from one month before to three months after these events. The average AO value 1 month before and two months after the event is slightly negative. Coinciding with the event and one month later the AO value is positive. Only AO-values 1 month after the event are above 1 standard deviation of the means found in the Monte Carlo-simulation, but the same month AO have values above this treshold within 1 standard deviations of the six events.

Based on these calculations, we find that the Ap- and AO-indices are weakly correlated only during wintertime. The correlations of the Ap- and AO-indices are not improved by adding a simple 1-month or 2-month lag, but the lag itself could possibly have a seasonal

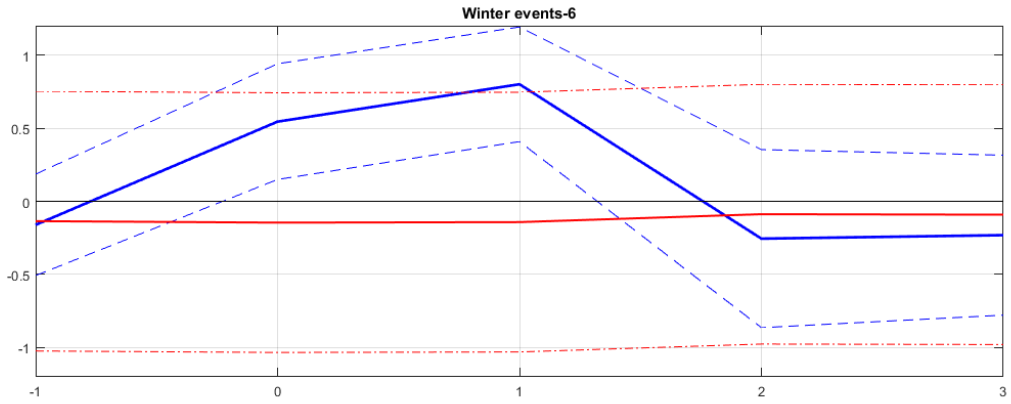

Figure 4.3: The AO-index following a high Ap-event shown in blue with error bars. The red lines are the mean of the Monte Carlo simulations with standard deviations.

variation making early events more likely to impact after 1 month whilst later events impact the AO-index the same months as the event.

4.2 MERRA-2 Climatology

4.2.1 Positive AO-characteristics

The MERRA-2 temperature data were used to create climatologies for positive AO-index values to compare with our findings for high activity periods. A positive AO means a strong, undisturbed polar vortex, as mentioned earlier. Figure 4.4 illustrates the temperatures of a positive AO-index compared to the total climatology at four different levels, 1000 hPa (≈ground level), 850 hPa (≈1.5km), 10hPa (≈30km) and 1 hPa (≈50km), to see effects at ground level, lower troposphere, middle stratosphere and upper stratosphere respectively. At ground level, a small region of elevated temperatures is visible over Northern Europe and Siberia, along with a cold region over Greenland and North America in November. These temperature anomalies grow in size over the winter season in both amplitude and extent. The cold temperature region above the Bering strait disappears, and the temperatures show a positive anomaly in February. These changes are also reflected at 850 hPa, though at a smaller amplitude. At10 hPa a warm region is visible over the North Atlantic in November, moving towards North America and growing in amplitude

in December, along with an extensive region of negative temperature anomalies over northern Europe and Siberia. In January the cold signature stretches across the North Pole towards North America before receding in February, giving way to positive temperature anomaliesl over Greenland, North America and the Arctic Ocean. At 1hPa a weak positive temperature anomaly is visible, growing in amplitude over the season. In February, it is located fairly symmetric around the North Pole with a warm anomalies 5 K above the climatology.

4.2.2 QBO, SSW and Volcano year characteristics

Temperature anomalies associated with other atmospheric phenomena are also interesting in order to understand the impact of potential biases in our analysis. Figure 4.5 illustrates the temperature anomalies of the SSW years (left), QBO westerly (middle left) and easterly (middle right) phase years, and years with volcano eruptions (right). These temperature differences are taken at four levels, similar to the positive AO-anomalies, but are only taken as mean values over December, January, and February for simplicity.

The SSW years at ground level are characterised by elevated temperatures above Greenland and North America, cold temperatures above northern Europe, Siberia and the Arctic sea, with a similar signature at 850 hPa. In the middle stratosphere (10 hPa) there is a distinct warm region above the North Pole and Greenland, stretching across Siberia. In the upper stratosphere (1 hPa) we see an extensive, almost circular region of cold temperatures, consistent with the theory in Chapter 2.2.5. As a positive AO-index indicates strong polar vortex and these signals show opposite tendencies, they seem to indicate a weak polar vortex, as expected.

The phases of the QBO show opposite signatures to each other. The westerly phase is characterised by a warm region above Siberia and the Bering Strait and a cold region above the pole along with a weaker cold signature above North America. At 850 hPa, the signature is similar, but the warm anomaly above the Bering Strait is stronger and more spread out, and the warm anomaly above Siberia is located further east. In the middle stratosphere (10 hPa) there is a cold region over the North Pole, while in the upper stratosphere (1 hPa) there is a warmer than average circular region above the North Pole. The easterly phase is characterised at ground level by colder northern Europe and Siberia

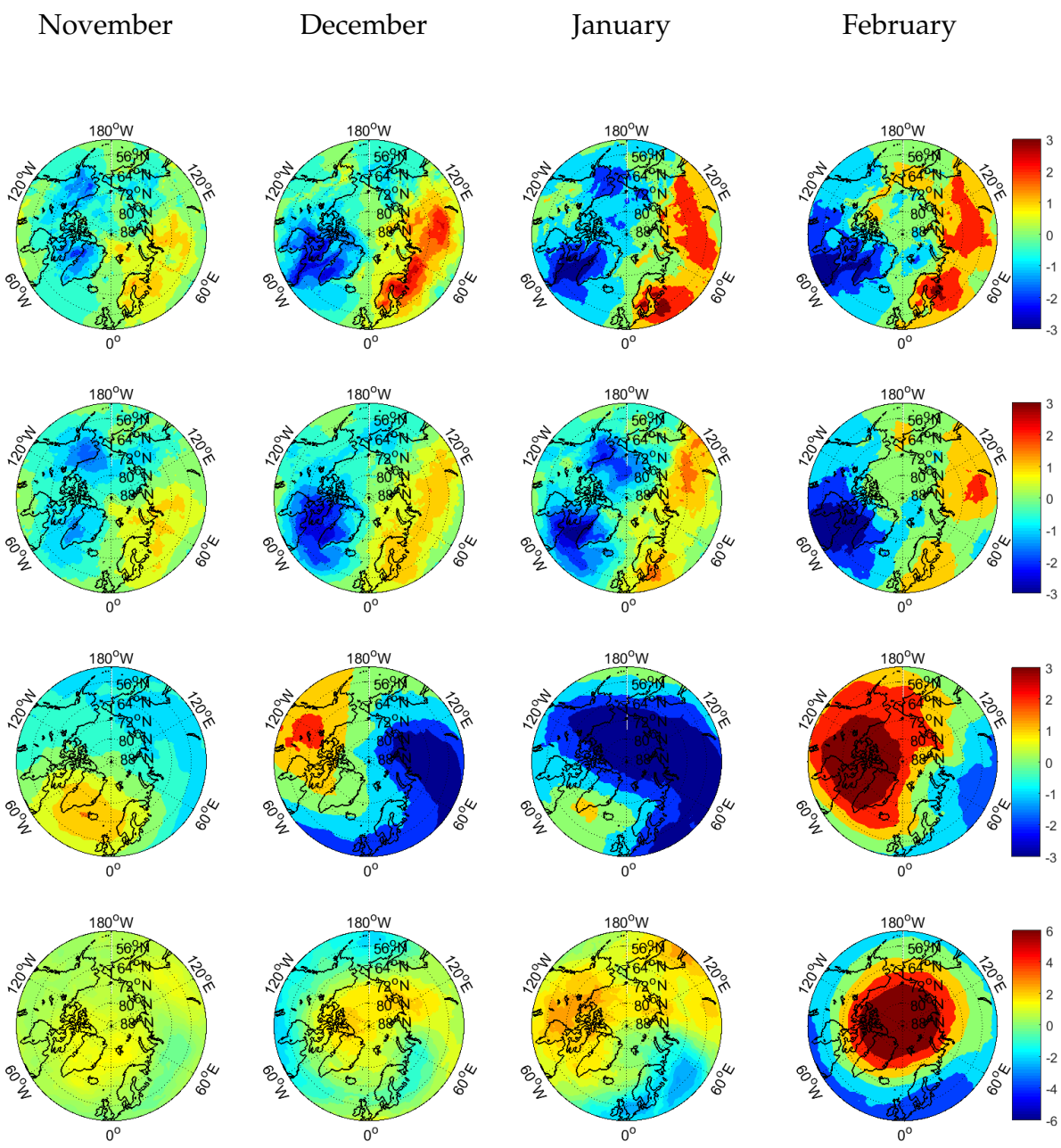

Figure 4.4: Pattern of a positive AO-index from November (left) to February (right) over four pressure levels, 1000 hPa (top), 850 hPa (middle top), 10 hPa (middle bottom) and 1 hPa (bottom). The unit for the colorbar of this figure and following similar figures is given in K.

as well as colder temperatures over the Bering strait and Alaska, with warm temperature anomalies over Greenland and eastern North America. At 850 hPa the signatures are similar to surface level signatures. At 10hPa a warm anomaly is seen over the pole and Siberia, whilst at 1hPa a cold anomaly is seen over the North pole, along with a weak heating over the North Atlantic. Westerly QBO shows signatures of a strong polar vortex, whilst the opposite ist true during easterly QBO. The easterly QBO signatures are very similar to the sudden stratospheric warming signatures. The magnitude of the QBO is smaller than that of the SSW.

The volcano years show signatures with comparatively higher amplitudes, with warm temperature anomalies of up to 5 K above Siberia and cold temperature anomalies of down to -5 K above Greenland and the Barents Sea. 850 hPa show similar, though slightly weaker, signatures. At 10hPa a strong warm temperature signature is seen over most of the Northern Hemisphere, whilst at 1hPa a strong warm temperature signature is visible above the North Pole and Greenland, stretching down towards the North Atlantic. There are only a two years of volcanic activity, in addition to the following year, in the time period studied, and they will therefore not be considered further.

4.3 Separation in high and low activity years

As mentioned in Chapter 3.1, we define high activity as months with an Ap-index exceeding the 55th percentile, and low activity in months with an Ap-index below the 45th percentile. We compare the high activity temperature climatology to both the all year climatology, and to the low activity temperature climatology. A student's t-test is run to determine the significance of the temperature signatures.

4.3.1 No time lag

Figure 4.6 show the temperature anomaly of high activity years compared to the total climatology for November to February at the four pressure levels 1000 hPa, 850 hPa, 10 hPa and 1 hPa. At ground level a small significant cold temperature anomaly is visible over northern Europe and the northern Pacific Ocean in November. In December, a significant warm anomaly is observed in December above parts of northern Europe and Siberia, with

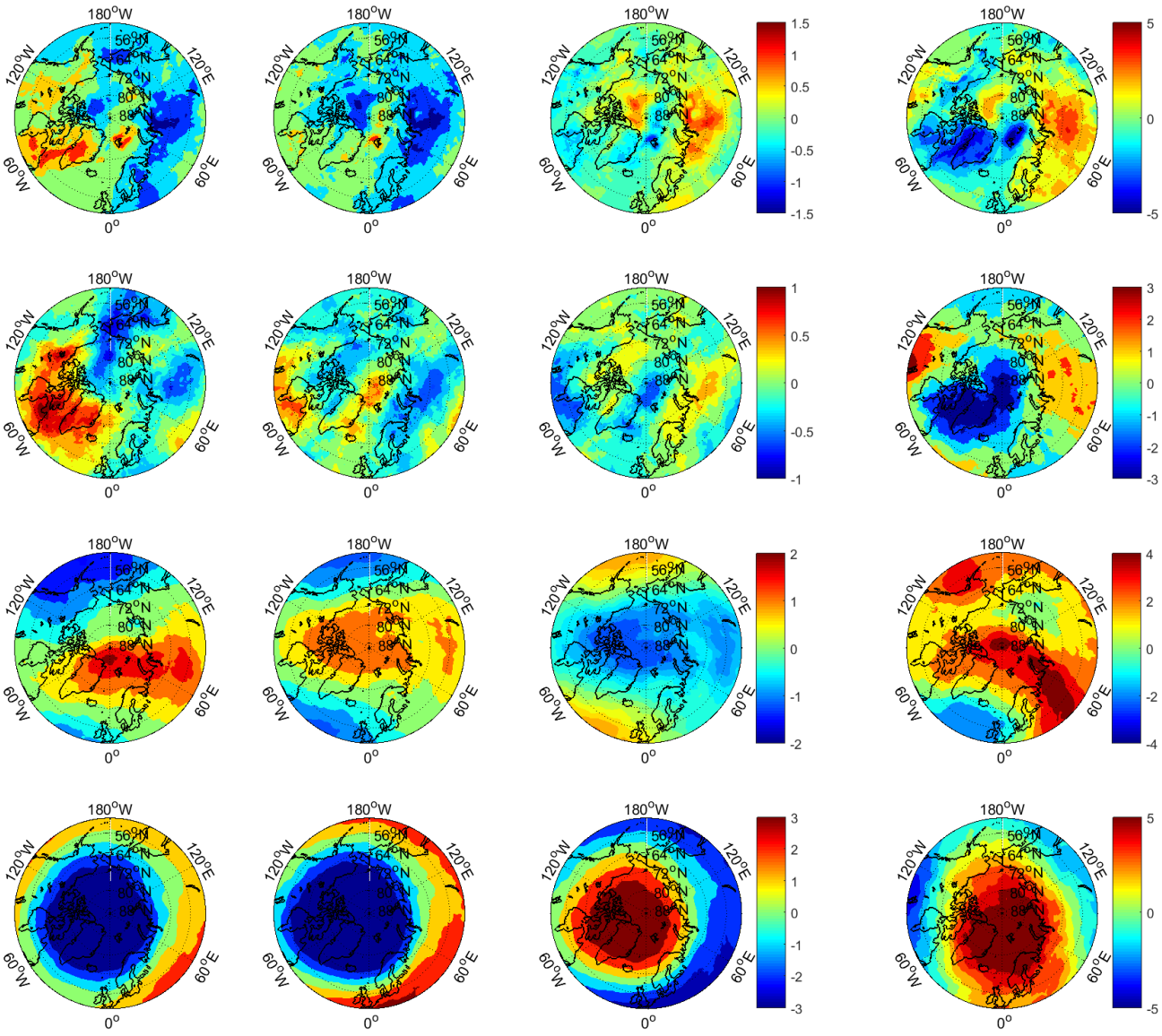

Figure 4.5: Wintertime temperature anomalies for SSW years (left), easterly QBO years (middle left), westerly QBO years (middle right) and volcano years (right). SSW and the QBO phase years use the same scale, and the volcano years use a separate scale.

non-significant cold temperature anomalies between Greenland and North America and above the pole. In January the signature is similar, but more significant above Siberia. The elevated temperature signature migrates eastwards and northwards towards the Bering Strait in February, and the cold anomaly becomes larger and more significant over North America. At 850 hPa the signature is generally the same, but less significant with the exception of February where significant regions covers eastern Siberia and eastern North America creating a distinct dipole-like signature. At 1 hPa a warm temperature signature is seen above the North Pole, becoming significant in December before dissipating in January. The warm signature reappears in February. The maximum amplitudes of these signatures are approximately ± 2.5 K at ground level and lower troposphere, approximately ± 4 K in the middle stratosphere and approximately ± 6 K in the upper stratosphere. At ground level and in the lower troposphere, the signatures are similar to the positive AO-index signatures with the exception of February. In the middle stratosphere, the cold temperature signatures are countered by warmer temperetures not visible in the positive AO in January and February, and the warm anomaly at 1hPa is stronger than the anomaly associated with the positive AO-signature in January.

When the high activity years are compared to the low activity years a similar, but stronger and more significant signature is observed at ground level. The signature becomes significant in December with a warm anomaly above northern Europe and Siberia, growing in amplitude and migrating north- and eastwards in February, and a cold anomaly above Greenland and North America and the North Pole, extending westward into Alaska in February. The warm temperature signature has a larger significant presence above western Siberia and northern Europe while comparing to low activity than compared to the total climatology, and the cooling signature is significant from Greenland to Alaska. At 850 hPa the elevated temperatures above Europe and Siberia is visible in December, but weaker than at the ground level, the same applies to the cold temperature signature above Greenland and North America. In January the warm temperature anomaly has migrated to central Siberia, and in February it has migrated to eastern Siberia, again creating a dipole-like structure with the cold anomaly above North America. At 10 hPa a warm signature over the north Pacific Ocean appears in January. The wam anomaly migrates inland to North America in January before covering the whole polar region in February. At 1 hPa we see a ring-shaped region of elevated temperaturesl stretching around the hemisphere, solidifying into a single warm anomaly above the North Pole in December. The elevated temperatures moves southward over Greenland, northern Europe and Siberia in January

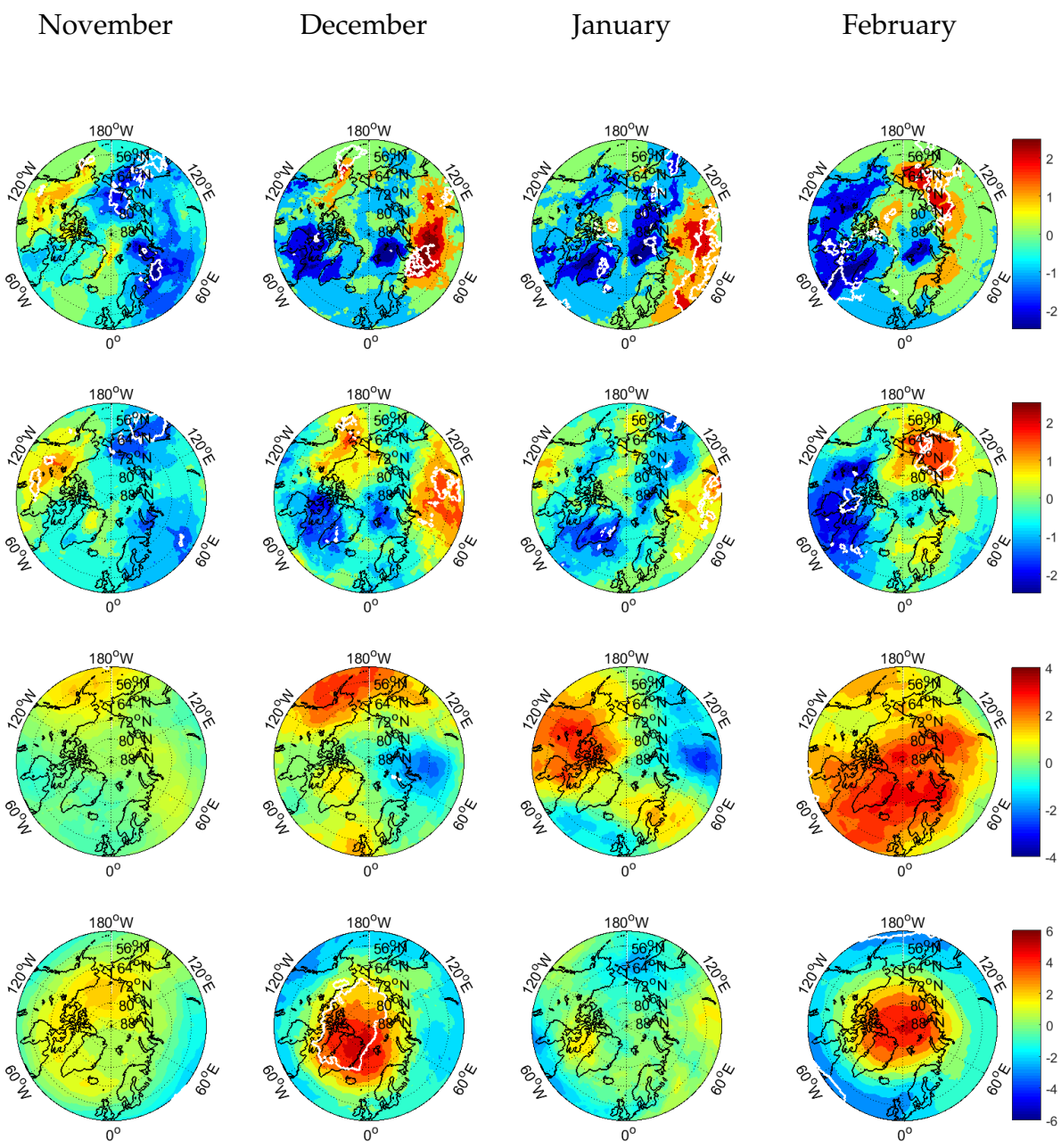

Figure 4.6: High activity years temperature difference to total climatology, from November (left) to February (right), at four levels, 1000 hPa (top), 850 hPa (top middle), 10 hPa (bottom middle) and 1 hPa (bottom). The white lines show significance at the 5% level.

before again settling as a close to circular region of warm temperature anomalies above the pole in February. The maximum amplitudes of these signatures are approximately ± 6 K on all three levels. These signatures are illustrated in Figure 4.7.

When SSW-years are removed, the same characteristic signatures are visible, as illustrated in Figures B.3 and B.4, found in Appendix B. The ground level and lower troposhere signatures are stronger and more wide-spread in December. In January the signatures are virtually identical, and in February the SSW year signature does not migrate eastward and is weaker and non-significant. Both the middle and higher stratosphere heating signals are stronger until February, where they are slightly weaker in the case of middle stratosphere, and completely gone in the case of upper stratosphere.

4.3.2 One month lag

With one month time lag, significant temperature anomalies are not visible until January, which then are nearly identical to the non-lagged signatures. In the lower troposphere (850 hPa), the anomalies are also not visible until January, but being slightly stronger than non-lagged signatures. February give approximately the same signatures as with no lag. At 10 hPa, the warm anomalies are more spread out, more significant and have larger amplitudes except in February, were it is slightly less spread out. At 1 hPa a significant slightly ring-shaped warmer region is visible stretching almost around the whole hemisphere. This warm anomaly migrates above Siberia in December, with a cold anomaly appearing south of Greenland. See Figure 4.8 for comparison with low activity years. To see comparison to total climatology, see Figure B.5 in the appendix.

4.4 High activity impact within atmospheric phenomena

Although not identical, the apparent temperature signature resembles the positive AO-climatology. In this section we will investigate to what extent our result is biased towards atmospheric phenomena such as the SSW and QBO. To avoid aliasing towards a phenomenon, temperatures from high Ap-years in SSW-years, QBO westerly phase years and QBO easterly phase years were compared to low activity years in the same group as well as the total climatology (including years not in the same group). When comparing the

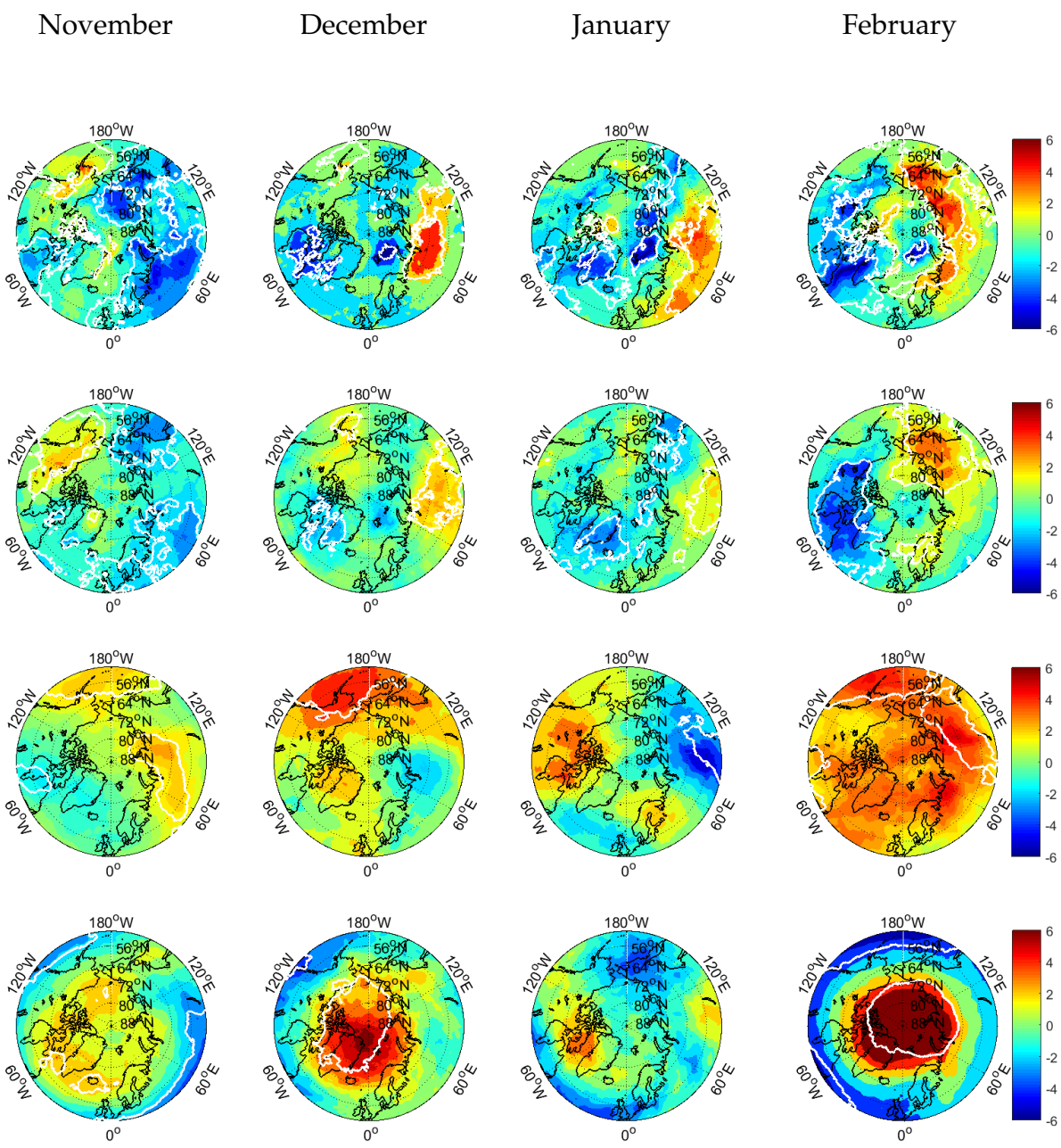

Figure 4.7: Similar to Figure 4.6, but compared to low activity years. The white lines show significance at the 5% level.

high and low activity years during the years of f.ex. easterly QBO phase, neither the low activity nor the high activity years will be biased toward the QBO phases when comparing

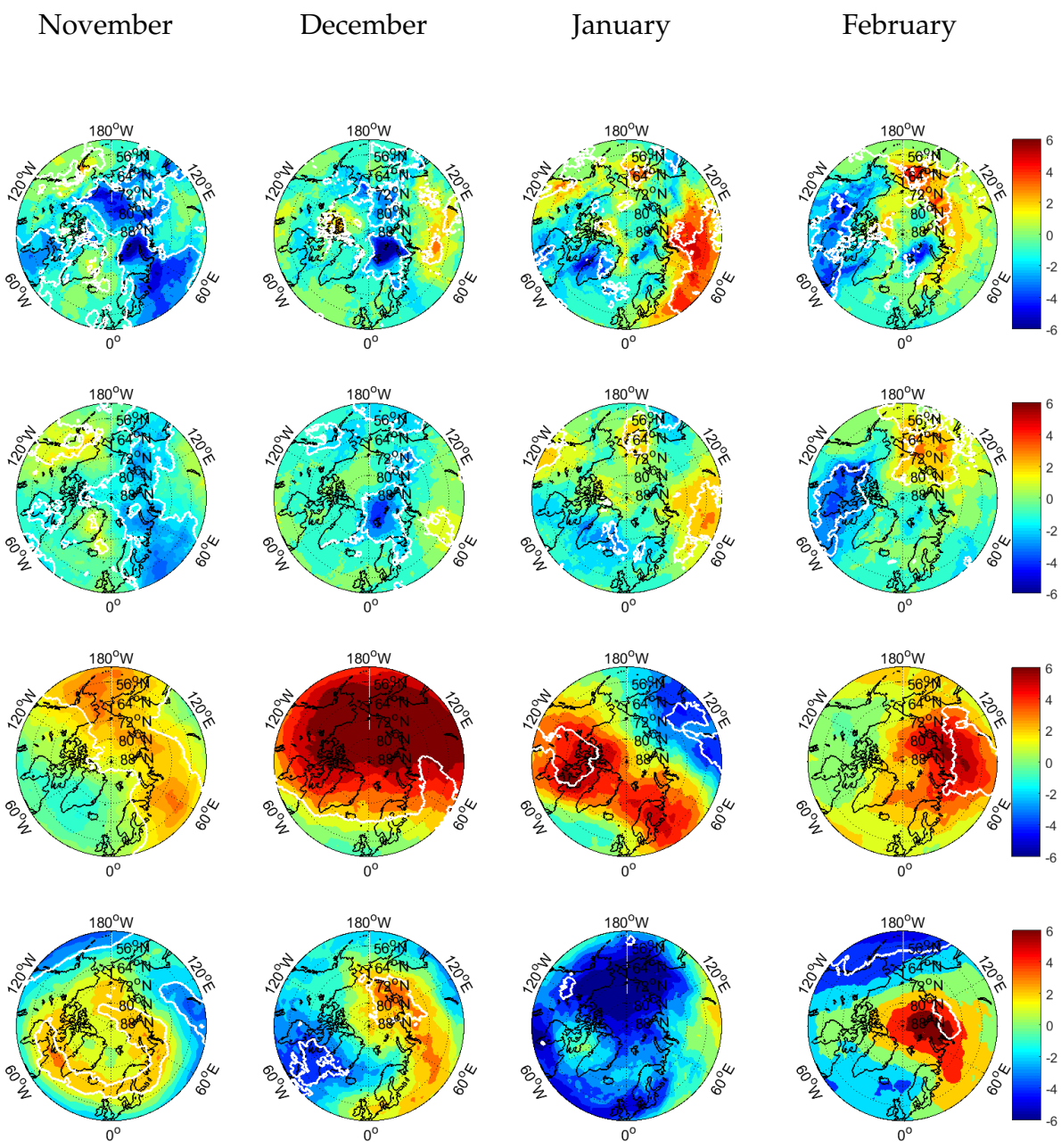

Figure 4.8: Temperature difference from high activity to low activity with one month lag, from November (left) to February (right), at four levels, 1000 hPa (top), 850 hPa (middle top), 10 hPa (middle bottom), and 1 hPa (bottom). The white lines show significance at the 5% level.

to the total climatology of f.ex. the QBO easterly phase. These tests are run at four pressure levels, similar to before, and are average values over December, January and February for simplicity. Within the SSW years, 4 years had high geomagnetic activity, with 10 years of low activity. For the easterly QBO, 6 years had high activity and 9 years had low activity. For the westerly QBO, 10 years had high activity and 7 years had low activity. See Figure 4.5 for the characteristics of the different phenomena.

Figure 4.9 illustrates westerly QBO phase years. Comparing high activity years to low activity years results in a strong significant cold temperature anomaly above Greenland and the Barents sea and a warm anomaly above Siberia at ground level. These signatures have maximum amplitude of approximately ± 4 K. At 850 hPa we see a large significant cold temperature signature above Greenland, the North Pole and the Barents sea, along with warm temperature signatures over Siberia and North America and a cold temperature signature in the pacific, creating four "poles". Maximum amplitudes are approximately ± 1.5 K. At 10 hPa, elevated temperatures are seen stretching from North America via Greenland to northern Europe, along with a cold temperature anomaly stretching from Siberia and into the Barents sea and a warm temperature anomaly in the Pacific. At 1 hPa significant warm anomalies are observed over the North pole, with cold anomalies at lower latitudes. These signatures have maximum amplitudes of approximately ± 3 K. When high activity western phase QBO-years are compared to the total climatology the signatures are similar to the comparison with low activity comparison, and generally show the characteristics of a strengthened westerly QBO.

Figure 4.10 shows the anomalies in easterly QBO. The high activity easterly QBO-phase years compared to the low activity years of the same group show significant elevated temperatures above Siberia and the north Pacific along with colder regions above Greenland, North America and the Barents sea. The cold signature in this phase is stronger than the westerly phase years, but the warm signatures are less spread out. Maximum amplitudes are approximately ± 4 K. At 850 hPa we observe a band of cold temperature anomalies from North America, via Greenland to northern Europe which is significant above most of North America. A small significant warm signature is visible in Siberia along with a warm anomaly above the Bering strait. Maximum amplitudes are approximately ± 1.5 K. At 10hPa a strong elevated temperature signal is visible above North America with maximum amplitudes of approximately 4 K. No significant cold anomalies are visible. At 1 hPa significant cold anomaly is visible over the North Atlantic, accompanied by non-

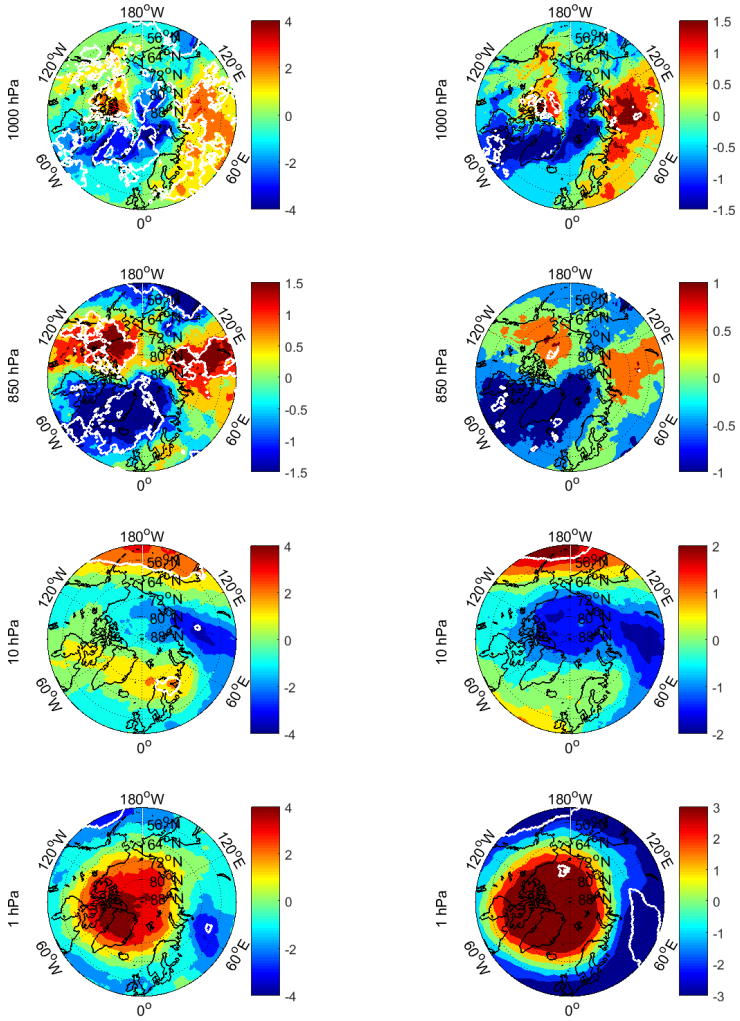

Figure 4.9: High activity westerly QBO year anomalies with regard to low activity years in the same group (left) and total climatology (right). The white lines show significance at the 5% level.

significant areas of lower temperatures over the Pacific Ocean and elevated temperatures over Siberia and North America, with maximum amplitudes of ± 4 K. When comparing to total climatology, a significant cold anomaly is visible above North America at ground level and 850 hPa, opposite of its normal characteristics. At 10hPa, a warm anomaly is

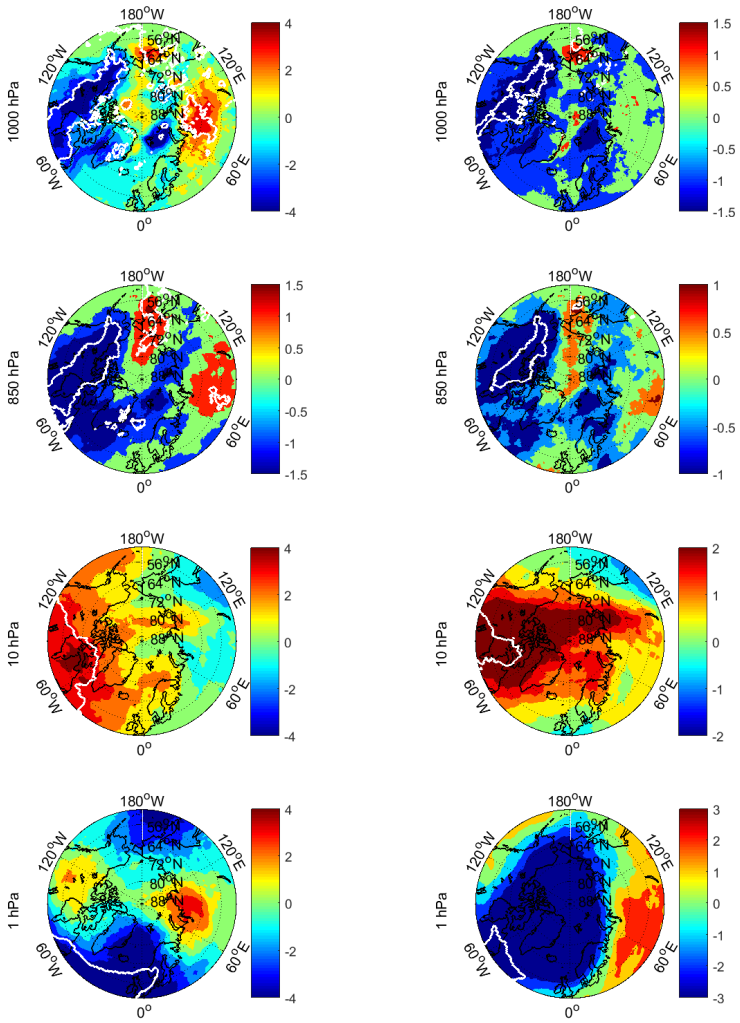

Figure 4.10: High activity easterly QBO year anomalies with regard to low activity years in the same group (left) and total climatology (right). The white lines show significance at the 5% level.

visible above North America, stretching across the North Pole towards Siberia. This is significant above North America, and looks similar to the normal easterly QBO, with the warm anomaly moved further inland in North America. At 1 hPa, the signatures are fairly similar to the normal easterly QBO signatures.

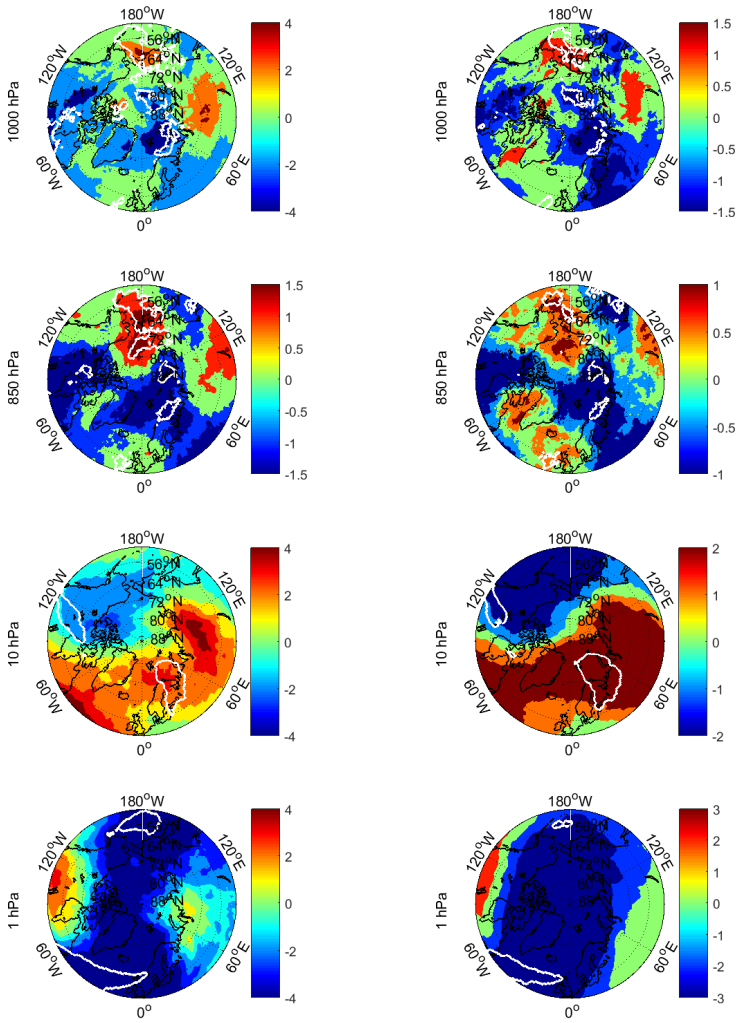

Figure 4.11: High activity SSW year anomalies with regard to low activity years in the same group (left) and total climatology (right). The white lines show significance at the 5% level.

Figure 4.11 shows the anomalies of SSW years.At ground level, high activity sudden stratospheric warming years show small significant cold anomalies above the Barents sea and North America accompanied by a small area of significant warm anomalies above the Bering strait and a non-significant warm anomaly above Siberia when compared to low

activity years of the same group, with maximum amplitudes of approximately ± 4 K. At 850 hPa, a large, partly significant cold anomaly stretching from North America, across Greenland towards northern Europe is visible, with significant elevated temperature signatures visible above the Bering strait accompanied by non-significant elevated temperatures above eastern Siberia. Maximum amplitudes are ± 1.5 K. At 10 hPa, warm signatures stretch from the North Atlantic, across northern Europe and into Siberia, being significant at a small area north of Russia. A cold anomaly is visible above North America. At 1 hPa we see cold anomalies above most of the polar region, with small non-significant warm anomaly above North America and Siberia. Maximum amplitudes are ± 4 K. Comparing to total climatology, the signatures are generally similar to the ones compared internally in the SSW years, but with higher amplitudes. The ground level and 850 hPa signatures are approximately opposite to the characteristics of a normal SSW year, but the middle and upper stratosphere looks similar to normal SSW years.

In general, the same signatures are visible throughout most of the atmosphere when compared internally in an atmospheric phenomena as when looking at all years. The high activity characteristics are strong enough to be visible at ground level even through dampening effects of the SSW and easterly QBO compared to total climatology.

5 Discussion

In this section, the results found will be summarised and compared to previous results. Possible errors and sources of aliasing will be listed. Finally, a discussion of the potential mechanisms by which EPP-induced NO_x and ozone perturbations could modulate stratospheric and tropospheric temperature patterns is included.

5.1 Summary of findings

This thesis examined the effect of EPP upon the arctic surface temperature during winter, both using the AO-index as a proxy and using the temperatures from the MERRA-2 reanalysis. It was found that the Ap-index shows a significant, positive correlation with the AO-index during winter. The mean December, January and February correlation of Ap- and AO-indices is 0.25 (p=0.04) in the period 1950-2016 and 0.29 (p=0.09) in the period 1980-2016. This effect is largest in December and January, with no significant correlation in February. A potential time lag between Ap and AO was investigated using simple correlation, as well as a super epoch analysis. The latter showed an indication of one month delay of AO-index compared to the Ap-index. The correlation analysis, however, implies that the specific time lag may vary throughout the winter.

When looking at the impact of high geomagnetic activity on MERRA-2 reanalysis data, significant warm anomalies over northern Europe and Siberia is observed, accompanied by cold anomalies above Greenland and North America. This effect grows in magnitude and extent over the winter, peaking in January with amplitudes of approximately 2 K when comparing to total climatology, and approximately 6 K when comparing to low activity periods. In contrast to the AO-correlation the effect is still significant in February, but the positive anomaly is placed more poleward and eastward. By comparing the AO-signatures in Figure 4.4 to the high geomagnetic activity signature in Figure 4.7, we see that the December and January high activity signatures are similar, but more confined than the positive AO-signatures. In February the signature has migrated eastward and thus lowering the Ap- and AO-correlation. Removing sudden stratospheric warming years increases ground level signatures in December and January, but gives weaker, non-migrating signatures in February, as shown in Figures B.3 and B.3 in the Appendix.

Assuming a lag of one month, the ground level signatures are similar, being stronger in January, but weaker the other months, as shown in Figure 4.8.

The ground level signatures do not seem to be biased by different atmospheric phenomena, and are visible through the SSW and easterly QBO years, changing their characteristics to that of the high geomagnetic activity characteristics. The westerly phase of the QBO is seemingly strengthened by high geomagnetic activity.

5.2 1950-2016 vs 1980-2016

As noted in Tables 4.1 and 4.2, the correlation between the Ap- and AO-indices during the years 1980-2016, which overlaps with the MERRA-2 reanalysis period, differ from the correlation in the decades before. In fact, while the Ap-index has a positive correlation with the AO-index after 1980, it shows negative correlation outside of the winter months in the time period 1950-1980, as shown in Table B.2 in the appendix. Whilst the AO-index tended towards negative values before 1980, the period 1980-2016 experiences a positive tendency in the AO.

Ozone plays an important role in the atmosphere as it shields the surface of the Earth from harmful solar UV-radiation. In the stratosphere, it also plays a critical role in the energy budget due to absorption of solar UV and terrestrial IR-radiation. Ozone in the troposphere acts as a strong greenhouse gas, and increasing ozone trends at these altitudes contribute to climate change. According to the *IPCC* [2013] report, global stratospheric ozone levels were reduced after 1980, particularily in the period before the mid-1990s. Since then, the ozone levels have remained nearly constant at approximately 3.5% below the pre-1980-levels. The ozone levels are changed primarily in the polar regions. The tropospheric ozone sees large regional trends. Northern Hemisphere has experienced an increase in surface level ozone of 1-5 ppb per decade, while the Southern Hemisphere increases are about 2 ppb per decade, in contrast to stratospheric ozone. Increases in the tropospheric ozone column were also observed over Southern Asia, as well as mid-latitude South and North Pacific Ocean since 1979.

The global mean surface temperature has risen since the late 19th century, with a marked increase in heating since the 1970s. The last three decades have all been warmer than any

decades preceding, going back as far as intrumental records go. Combined global land and ocean mean surface temperatures over the period 1880-2012 experienced a warming of 0.85 (0.65-1.06) K, while 1901-2012 experienced a warming of 0.89 (0.69-1.08) K and 1951-2012 experienced a warming of 0.72 (0.49-0.89) K [*IPCC*, 2013].

The sum of this is that the period of 1980-2016 differs significantly to the years preceding it, and any results might be difficult to generalise.

5.3 Potential aliasing effects

As the MERRA-2 reanalysis cover a rather low amount of years, it is not possible to account for all internal atmospheric variables when dividing into high and low activity years. Figure 5.1 illustrates our division of years, with westerly QBO noted in red, easterly QBO noted in blue, SSW years with italic text, and volcano years with bold text. Our definitions of QBO phase and SSW years is outlined in Chapter 3.4, and may differ from those used in other studies. The QBO phase and SSW have effects upon the polar ground level temperatures as well as stratospheric temperatures, and may as such impart a bias and potential aliasing effect upon our analysis.The number of high activity months vary between 14 and 17, whereas there are slightly more years (50%-62.5%) in the westerly QBO phase. We also note that the volcano years mostly fall in high activity years. In general SSW years are distributed fairly evenly, but there are slightly more SSW years for the low activity years during January and February compared to high activity months.

When high activity years were compared to low activity years within SSW and easterly QBO years, similar ground level anomalies as those found when looking at all years were found, however with lower amplitudes of ~1.5 K compared to ~4 K. The stratopause anomalies, show characteristics dissimilar to when looking at all years, showing cold anomalies over much of the polar region. This cold anomaly is more pronounced in the SSW years. The SSW and easterly QBO are known to disturb the vortex, and the strength of the vortex is thought to be important to the effect of EPP. *Seppälä et al.* [2013] suggest in fact that the EPP-impact on planetary wave propagation tends to take place when the stratospheric background flow is relatively stable, or where the polar vortex is stronger in early winter, as is the case for westerly QBO. As the ground level signatures still visible internally within the easterly QBO phase or SSW years themselves, it appears that the

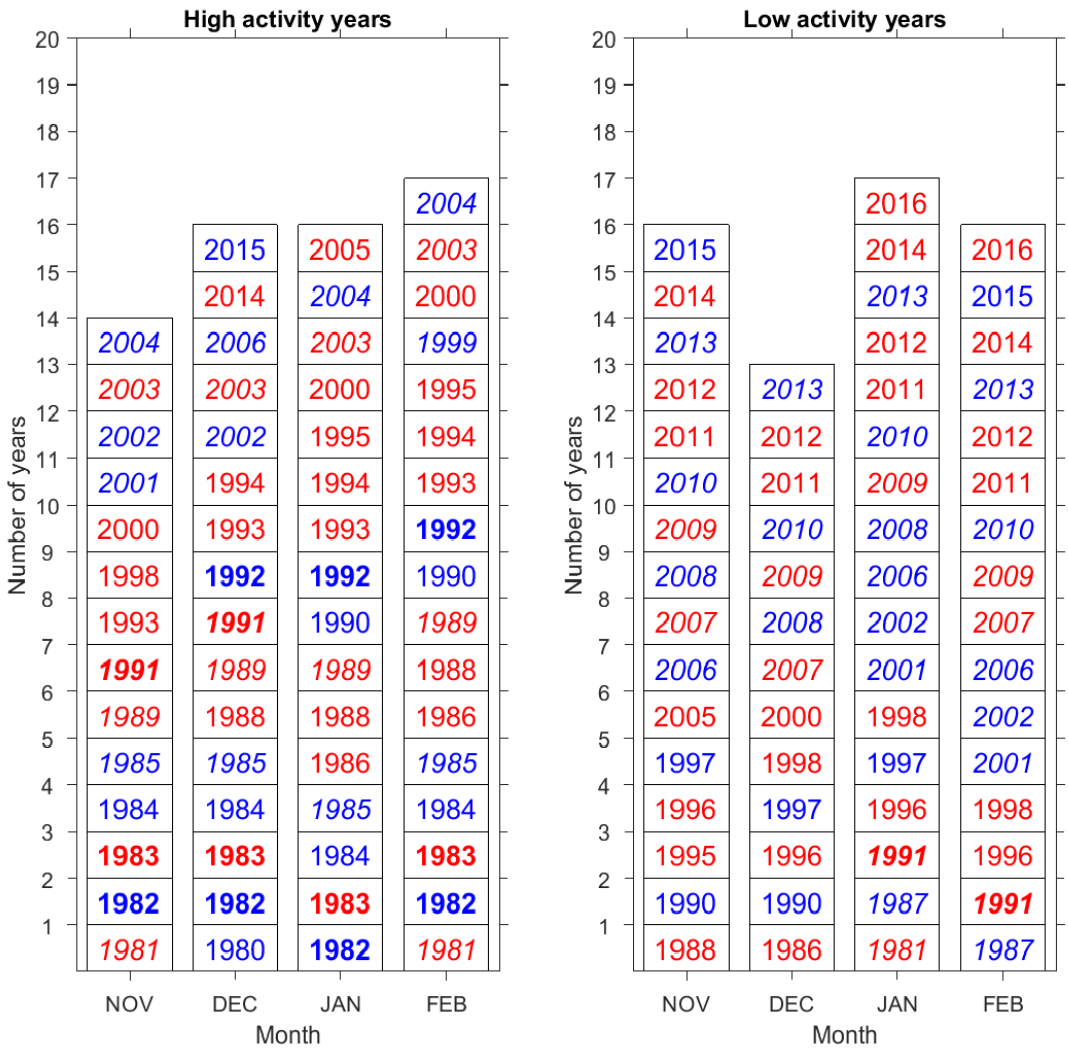

Figure 5.1: Years of high (left) and low (right) activity for months studied. Years in red are westerly QBO, years in blue are easterly QBO. Years with bold font are years of volcanic activity, and years with italic font are SSW years.

signatures are not caused solely by an aliasing effect caused by SSW or the phase of the QBO. Note, however, that volcano years are still part of the high activity years focusing on the QBO phases.

As mentioned in Chapter 2.3.2, increases in UV-radiation brings similar dynamic responses and temperature anomalies as EPP. While *Seppälä et al.* [2013] divided into high and low UV-radiation as well as EPP to separate the effects, this was not done in this thesis. As

such, the years of high solar irradiance may impart also a bias upon our findings.

5.4 Results with respect to previous studies

This thesis uses monthly averaged Ap as a proxy to determine fluxes of EPP, analogue to *Seppälä et al.* [2009]. Monthly averages does not provide information of the variability within the interval. A large storm typically lasts 1-3 days, and the monthly averaged Ap-index will not differentiate between long-lasting moderate storm or isolated high intensity storms. It also does not take into account whether a storm occurs early or late in the time interval being averaged, as pointed out in Chapter 3.1. It should also be noted that our high activity months, in particular February, have a strong bias towards the period 1980-1995, as evident in Figures 3.3 and 5.1.

Maliniemi et al. [2013] noted that the Ap-index is a rather crude proxy for the electron fluxes at higher energies, as demonstrated in Figure 3.2. Investigating the correlation between the three months average electron fluxes with NAO at 500 hPa, they achieved a correlation of 0.44 ($p = 0.015$) for 30-100 keV electrons, and 0.44 ($p = 0.031$) for 100-300 keV. By excluding some strong SSW years, the correlations were increased to 0.64 with p-value < 0.001 and 0.65 with p-value < 0.001, respectively. These results suggest that a better correlation could be found with a more accurate proxy for the EPP forcing. *Lu et al.* [2008] found strong correlation (up to 0.8) between solar wind dynamic pressure and and the NAM index at 150 hPa (~13 km) calculated from ERA-40 reanalysis data for January to February, but only when years of high F10.7 flux were considered. Hence, the strong correlation might not just be due to solar wind dynamic pressure being a better proxy than Ap, but that the potential mechanism is strengthened by solar UV, as explained in Chapter 2.3.3.

Figure 5.2 shows our DJF anomalies compared to the anomalies found by the model simulations of *Rozanov et al.* [2005], the NASA Goddard Institute for Space Studies air temperature analysis data of *Maliniemi et al.* [2013] and the ERA-40 reanalysis data of *Seppälä et al.* [2009]. Their anomalies are mean values over December, January and February. When using mean values over the winter season, the February eastward migration of the warm anomaly is not visible, but the warm anomaly found in this thesis is otherwise consistent geographically with their anomalies. All three also observe cold anomalies close to Greenland, but the warm anomalies observed by *Rozanov et al.* [2005] over North

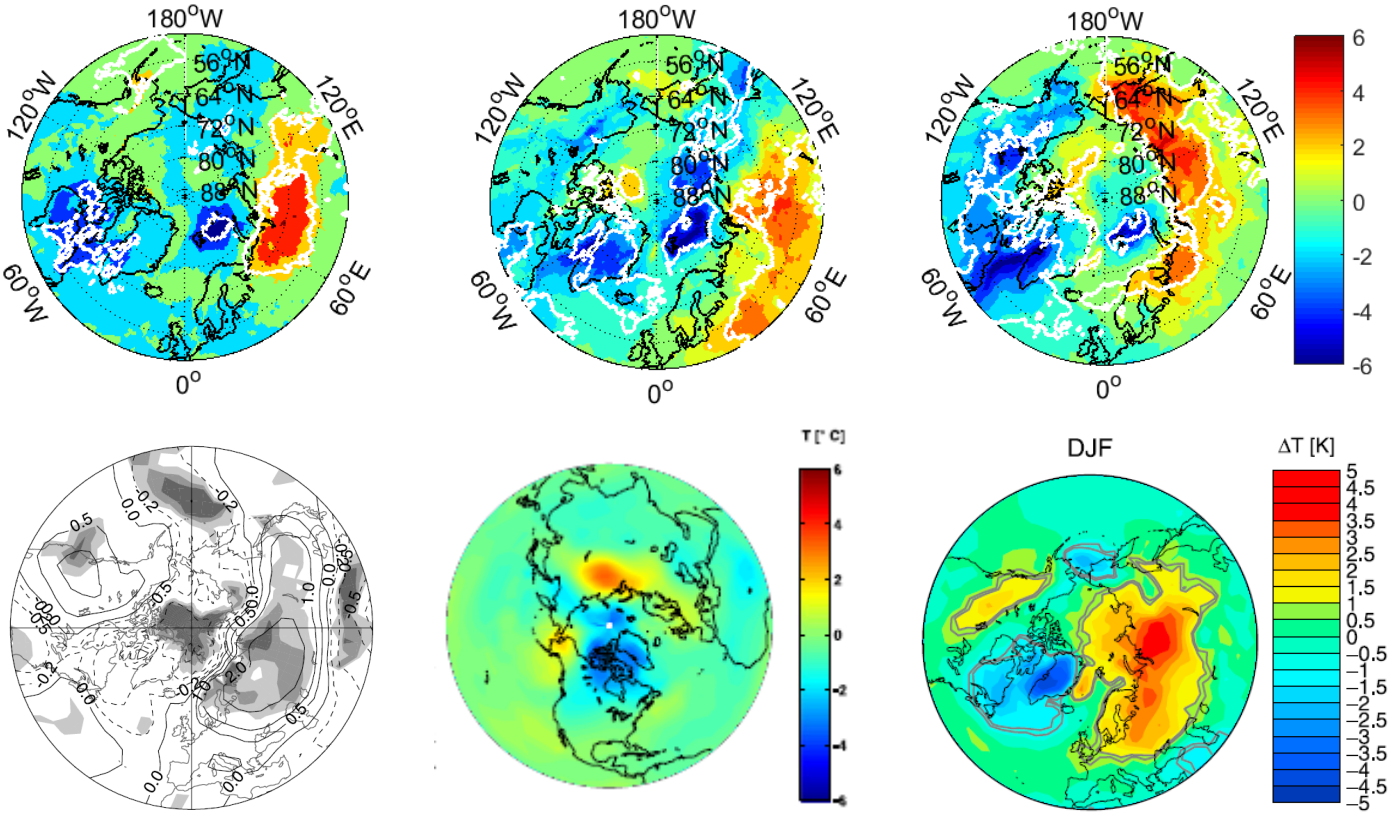

Figure 5.2: Our DJF anomalies from high activity years compared to low activity years, compared to the anomalies found by *Rozanov et al.* [2005] (lower left), *Maliniemi et al.* [2013] (lower middle) and *Seppälä et al.* [2009] (lower right).

America are only visible in January in our studies. Maximum amplitudes found by *Rozanov et al.* [2005] were ~2.5 K which are comparable to our high activity years compared to total climatology. When comparing high activity to low activity, we found temperature anomalies of up to 6 K, while *Seppälä et al.* [2009] and *Maliniemi et al.* [2013] found anomalies of up to ~5 K and ~6 K by contrasting high and low activity.

5.5 Mechanisms

This thesis does not apply data of chemical composition of the atmosphere, and as such we cannot directly verify that a reduction of ozone is observed at the stratopause levels. We do, however, observe temperature anomalies at different pressure levels corresponding

to middle (~30 km) and upper (~50 km) stratosphere levels.

Based on the model simulations performed by *Baumgaertner et al.* [2011], we expect a heating of up to 2 K averaged from December to February. This is due to reduction of ozone and the associated reduction in the infrared cooling rate contrasting high and low activity in the upper stratosphere. In the upper stratosphere we find significant heating relative to the climatology of $\tilde{4}$ K in December. There is also a positive non-significant anomaly in January and February. Contrasting high and low activity this amplitude reaches ~6 K, and becomes significant also in February. *Baumgaertner et al.* [2011] also predicted a cooling effect deeper into the stratosphere associated with a weakened mean meridional circulation causing less adiabatic heating. At 10 hPa we see a regional cooling effect significant in January. Heating seems, however, to be the main feature of this altitude as well, and we do not as such see any clear evidence of this dynamical effect. We speculate that 10 hPa might still be too high in the stratosphere to see this secondary effect.

Further, a positive AO indicates a strong polar vortex. The anomalies for high activity years at 10 hPa in Figure 4.6 are somewhat similar to the AO anomaly in Figure 4.4, at least with respect to the cold anomaly. Please note the different temperature scales in the figures. This cooling feature, although not significant, is also evident in the westerly QBO for high and low activity in Figure 4.9. The strengthened polar vortex affects ground level similar to the positive AO-anomalies, with a warmer Northern Europe and Siberia and colder North America and Greenland. The opposite stratospheric signatures is found when looking at high and low activity during the easterly QBO and SSW years, hence it does not seem to be a general feature associated with the high activity years.

In summary, if the suggested mechanism is real, it appears to be dependent on westerly QBO and a strong polar vortex to take place and be efficient. This confirms the previous hypothesis by *Lu et al.* [2008] and *Seppälä et al.* [2013] that strong vortex (due to either high solar irradiance or westerly QBO) makes the geomagnetic impact on the planetary wave propagation and the surface temperature more efficient. The fact that the geomagnetic activity and the surface temperature occur apparently without any significant lag may however cast doubts upon the suggested mechanism, as it is dependent upon travel time from mesopause levels and the dynamic response. No time lag limits the type of event that could have an impact, causing a bias towards high energy particles. Note that while the stratospheric signatures are very dissimilar for easterly QBO and SSW years, the

ground level signatures are fairly similar but with lower amplitudes. This might indicate a second or a different mechanism not dependent on QBO and SSW in addition to the chemical-dynamical coupling suggested by *Lu et al.* [2008] and *Seppälä et al.* [2013].

5.6 Other possible errors

Any scientific endeavour includes the possibility of errors. Here some possible sources of errors are listed.

Using reanalysis data brings sources of errors. The algorithms used might be flawed, and any measurements are only accurate to a certain level. Of particular note for MERRA-2 is the middle atmosphere bias above 10 hPa caused by change of instruments, as mentioned in Section 3.3, as well as the short time span covered.

When running a statistical analyses, the kind of analysis chosen and the way it is implimented might affect the results found. As such, a poorly chosen statistical method may lead to conclusions drawn on false premises. Although we are confident that the analyses used in this thesis are relevant, caution is always prudent. Correlation does not imply causality, and statistical outliers might occur where seemingly significant results are actually randomly occuring.

6 Conclusion and future work

In this section we will draw a conclusion based on our results and subsequent discussion. Suggestions for future work is included.

6.1 Conclusion

The Ap- and AO-indices are used as proxies for EPP and ground level temperatures, respectively, and a positive, significant correlation between monthly averaged Ap- and AO-indices is found. Also, MERRA-2 reanalysis data shows significant warm anomalies over northern Europe and Siberia, accompanied by significant cold anomalies of similar amplitudes at ground level in December, January and February the same month and one month after high geomagnetic activity. December and January signatures correlate well with the Arctic Oscillation-characteristics, and February shows similar features shifted eastward, all indicating a strengthened polar vortex and a lowered Brewer-Dobson circulation. These signatures have maximum amplitudes of up to 6 K when comparing to low activity years, or 2.5 K when compared to the total climatology. At stratopause levels heating is observed, in line with reduction of radiative cooling from ozone. Further analysis is required to reveal a potential dynamical induced cooling deeper into the atmosphere. Contrasting high and low activity easterly QBO, westerly QBO and SSW years, it is evident that only the westerly QBO years show the suggested warm stratopause anomaly. Hence, through our analysis hints at EPP surface impacts, a sound understanding of the mechanisms by which the EPP-induced NO_x and ozone perturbations could modulate stratospheric and tropospheric circulation patterns remains to be firmly established.

6.2 Future work

This thesis is not to be taken as a full study of the whole effect of high geomagnetic activity upon the atmosphere. There are for instance several atmospheric phenomena not discussed in length in this thesis, e.g. the ENSO, which could impact or bias the results. Other possible mechanisms linking stratosphere and ground level should be investigated through more detailed altitude resolutions and with more variables such as Eliassen-Palm

flux, zonal winds, etc.

As shown in Section 4.1, the time used from geomagnetic activity to surface signal might vary over the winter season. Determining the timing over the season, possibly on a daily or weekly scale, and determining exactly why the timing varies would be of interest to fully understand this phenomenon.

As of writing this thesis, precipitating particle fluxes are not well determined, and proxies are used in their stead. As proxies do not give the full picture of the situations described, it should be a priority to determine these particle fluxes to a greater extent.

A Glossary

Abbreviation	Full name
AO	Arctic Oscillation
CME	Coronal Mass Ejections
ENSO	El Niño - Southern Oscillation
EEP	Energetic Electron Precipitation
EPP	Energetic Particle Precipitation
GCR	Galactic Cosmic Rays
IMF	Interplanetary Magnetic Field
NAM	Northern Annular Mode
NAO	North Atlantic Oscillation
QBO	Quasi-biennial Oscillation
SAO	Semi-annual Oscillation
SPE	Solar Proton Events
SSI	Solar Spectral Irradiance
SSW	Sudden Stratospheric Warming
TSI	Total Solar Irradiance

Table A.1: List of abbreviations

B Additional figures and tables

In this section figures and tables not used in the thesis itself can be found.

Name	Source	Time range	Assimilation	Model Resolution	Reference
ECMWF Interim Reanalysis (ERA Interim)	ECMWF	1979-present	4D-VAR	T255, 60 Hybrid Sigma levels, 1000 hPa-0.1 hPa	*Dee et al.* [2011]
ECMWF 40-year Reanalysis (ERA-40)	ECMWF	1957-2002	3D-VAR	TL159L60 and N80 reduced Gaussian	*Uppala et al.* [2005]
CERA-20C	ECMWF	1900-2010	4D-VAR	T159, 91 model levels	*Laloyaux et al.* [2016]
Japanese 25-year Reanalysis (JRA-25)	Japan Meteorological Agency (JMA) and Central Research Institute for Electric Power Industry (CRIEPI)	1979-2004	3D-VAR	T106, 40 levels 1000 hPa-0.4 hPa	*Onogi et al.* [2007]
Japanese 55-year Reanalysis (JRA-55)	Japan Meteorological Agency	1958-Present	4D-VAR	T319, 60 levels, 1000 hPa-0.1 hPa	*Kobayashi et al.* [2015]
NASA MERRA	NASA GMAO	1979-2016	GEOS IAU	0.660 lon x 0.5olat, 72 Sigma Levels, 1000-0.1 hPa	*Rienecker et al.* [2011]
NASA MERRA-2	NASA GMAO	1980-present	3D-VAR, with incremental update; Includes aerosol data assimilation, observation corrected precipitation forcing for land surface and aerosol wet deposition	0.660 lon x 0.5olat, 72 Sigma Levels, 1000-0.1 hPa	*Gelaro et al.* [2016]
NCEP/NCAR Reanalysis I (R1)	NCEP/NCAR	1948-present	3D-VAR	T62, 28 Sigma Levels, 1000 hPa-3 hPa	*Kalnay et al.* [1996]
NCEP/DOE Reanalysis AMIP-II (R2)	NCEP/DOE	1948-present	3D-VAR	T62, 28 Hybrid Sigma Levels, 1000 hPa- 3 hPa	*Kanamitsu et al.* [2002]
NCEP Climate Forecast System Reanalysis (CFSR)	NCEP	1979-2011	3D-VAR	T382, 64 Hybrid Sigma Levels, 1000 hPa- 0.2 hPa	*Saha et al.* [2010]
NOAA-CIRES 20th Century Reanalysis (20CRV2c)	NOAA/ESRL PSD	1851-2014	Ensemble Kalman Filter	T62, 28 levels, 1000 hPa-10 hPa	*Compo et al.* [2011]

Table B.1: Table of global atmospheric reanalyses

Notes	Data sets	Correlation	p-value
All months, no time lag	1950-1980	0.12	0.01
Specific months, no time lag	Oct-Mar	0.16	0.42
	Apr-Sep	-0.59	0.01
	Dec-Feb	0.33	0.07
	Mar-May	-0.39	0.03
	Jun-Aug	-0.34	0.07
	Sep-Nov	-0.34	0.07
1 month lag	Ap Nov-Jan, AO Dec-Feb	0.28	0.14
	Ap Dec-Feb, AO Jan-Mar	0.24	0.20
2 months lag	Ap Nov-Jan, AO Jan-Mar	0.15	0.42
	Ap Oct-Dec, AO Dec-Feb	0.20	0.28
4 months Ap, 3 months AO, 2 months lag	Ap Oct-Jan, AO Dec-Feb	0.26	0.17
SSW years removed	All months, no time lag	-0.03	0.66
	Dec-Jan	0.17	0.50
	Ap Nov-Jan, AO Dec-Feb	0.13	0.59

Table B.2: Similar to Tables 4.1 and 4.2, but for 1950-1980

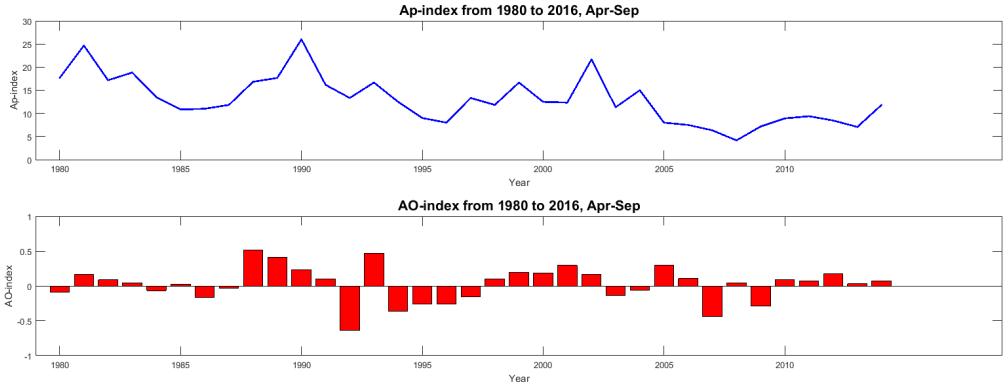

Figure B.1: Ap- and AO-indices from April to September 1980-2016

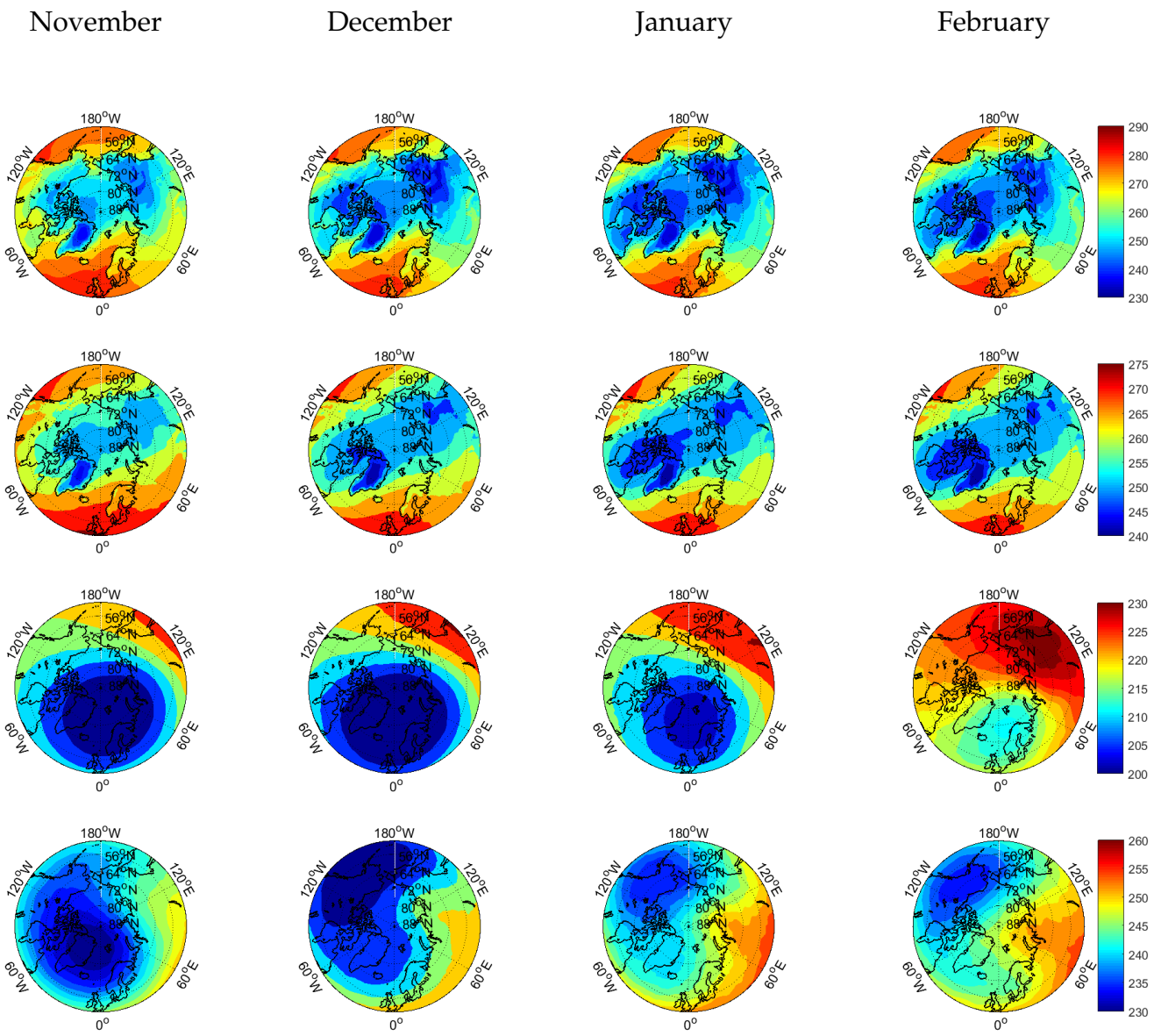

Figure B.2: Climatology of a positive AO-index from November (left) to February (right) over four pressure levels, 1000 hPa (top), 850 hPa (middle top), 10 hPa (middle bottom) and 1 hPa (bottom).

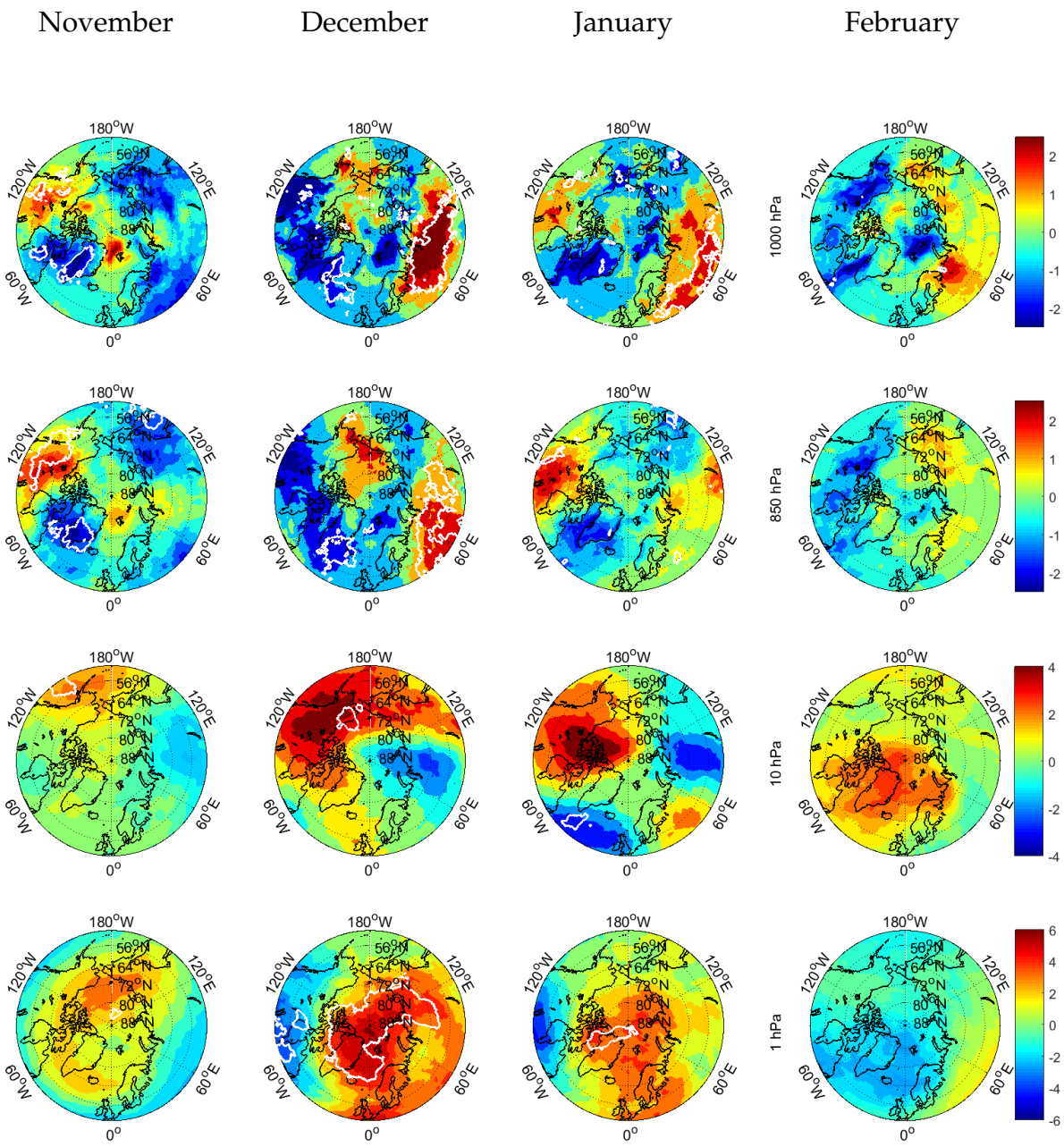

Figure B.3: High activity years temperature difference to total climatology with SSW years removed, from November (left) to February (right), at four levels, 1000 hPa (top), 850 hPa (middle top), 10 hPa (middle bottom) and 1 hPa (bottom). The white lines show significance at the 5% level.

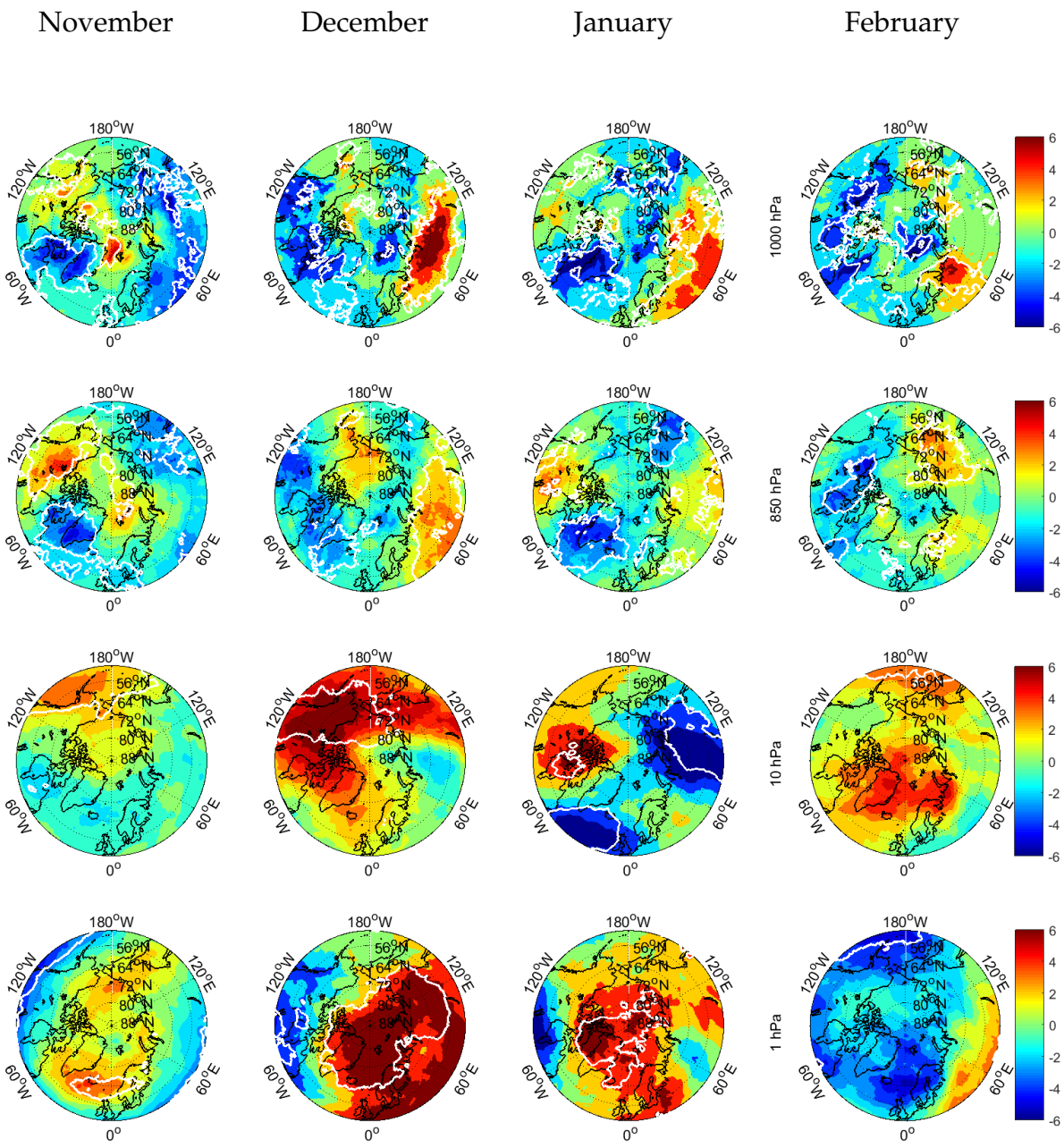

Figure B.4: Similar to Figure B.3, but compared to low activity years.

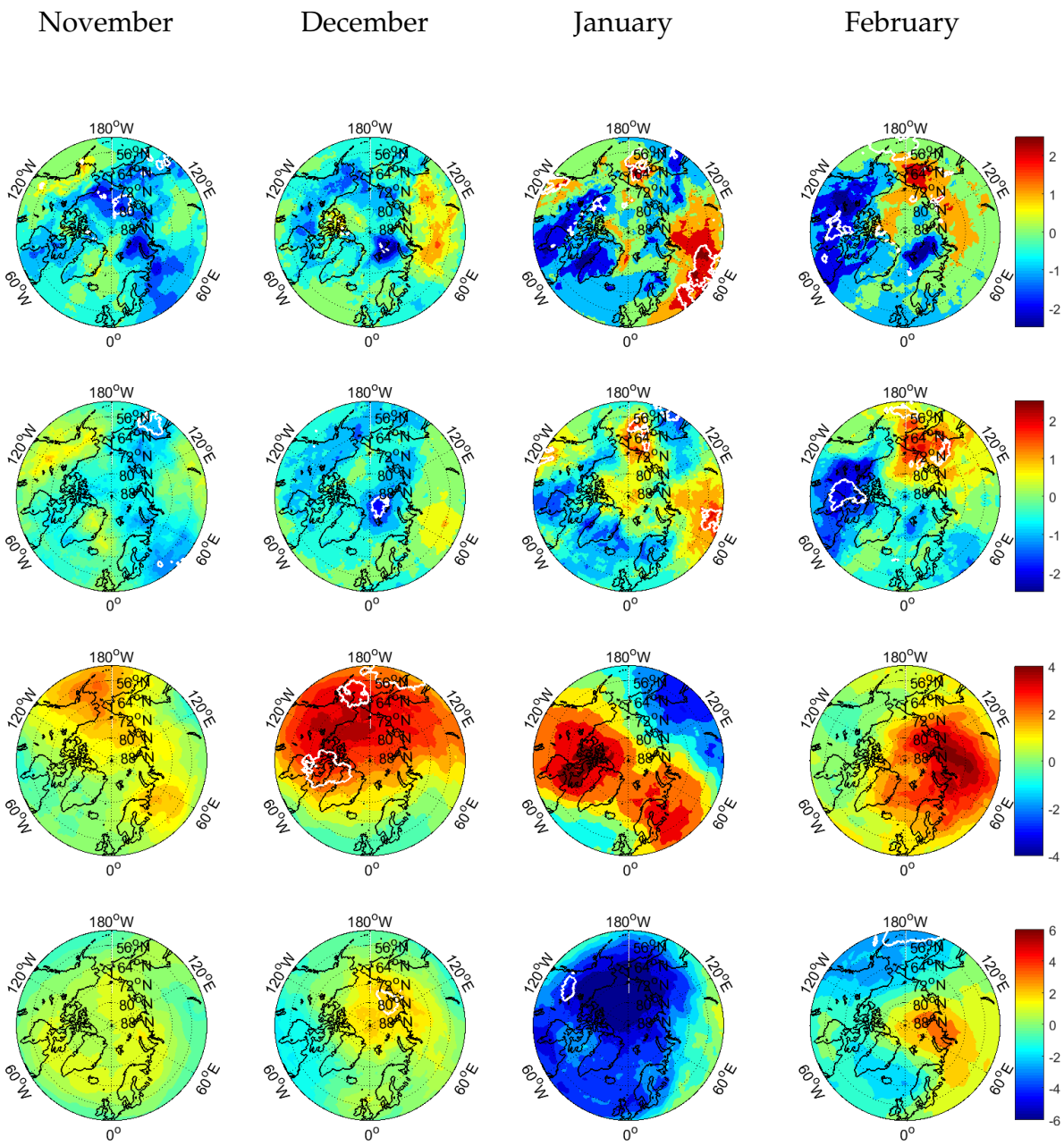

Figure B.5: Similar to Figure 4.8, but compared to total climatology.

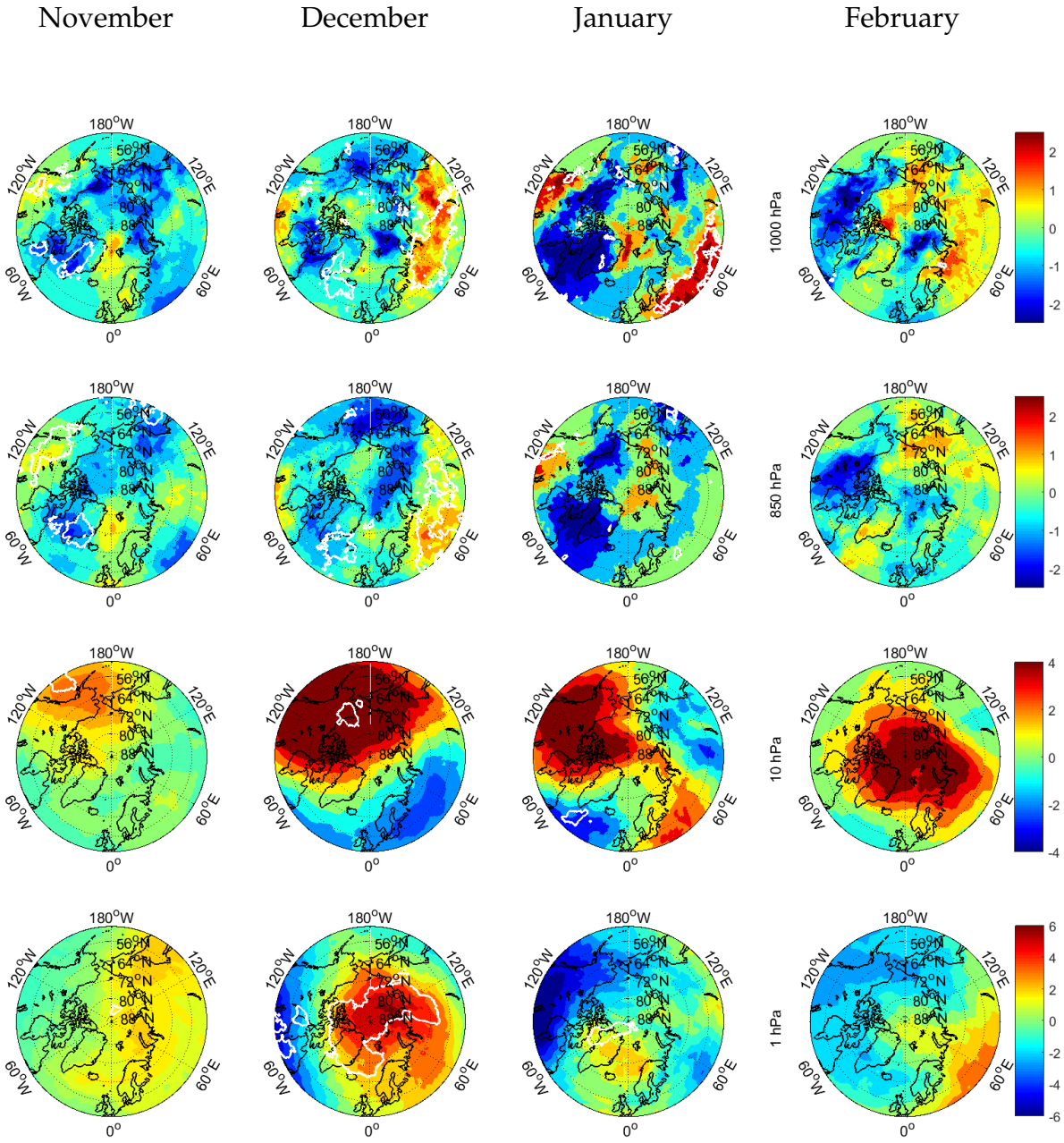

Figure B.6: Temperature difference to total climatology one month after high Ap, with SSW years removed, from November (left) to February (right), at four levels levels, 1000 hPa (top), 850 hPa (middle bottom), 10 hPa (middle bottom) and 1 hPa (bottom). The white lines show significance at the 5% level.

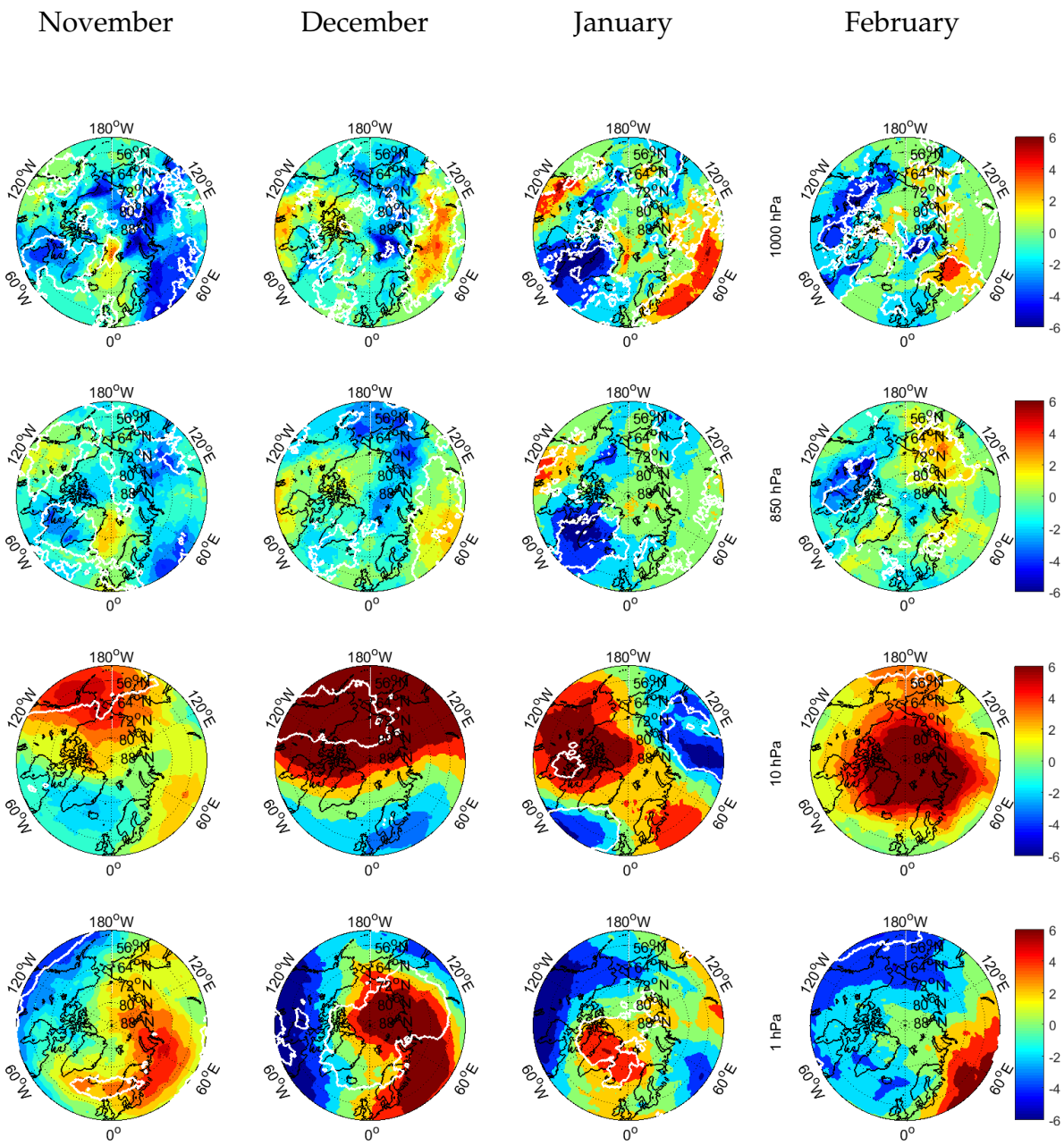

Figure B.7: Similar to Figure B.6, but compared to low activity years.

References

T. Asikainen and M. Ruopsa. Solar wind drivers of energetic electron precipitation. *Journal of Geophysical Research: Space Physics*, 121(3):2209–2225, 2016. ISSN 2169-9402. doi: 10.1002/2015JA022215. URL http://dx.doi.org/10.1002/2015JA022215. 2015JA022215.

M. P. Baldwin and T. Dunkerton. Stratospheric harbingers of anomalous weather regimes. *Science*, 294:581–584, 2001.

M. P. Baldwin, L. J. Gray, T. J. Dunkerton, K. Hamilton, P. H. Haynes, W. J. Randel, J. R. Holton, M. J. Alexander, I. Hirota, T. Horinouchi, D. B. A. Jones, J. S. Kinnersley, C. Marquardt, K. Sato, and M. Takahashi. The quasi-biennial oscillation. *Reviews of Geophysics*, 39(2):179–229, 2001. ISSN 1944-9208. doi: 10.1029/1999RG000073. URL http://dx.doi.org/10.1029/1999RG000073.

A. J. G. Baumgaertner, A. Seppälä, P. Jöckel, and M. A. Clilverd. Geomagnetic activity related NO_x enhancements and polar surface air temperature variability in a chemistry climate model: modulation of the NAM index. *Atmospheric Chemistry and Physics*, 11: 4521–4531, 2011.

G. P. Brasseur and S. Solomon. *Aeoronomy of the Middle Atmosphere*. Springer, third edition, 2005.

A. H. Butler, P. L. M., and C. Deser. Separating the stratospheric and tropospheric pathways of el niño–southern oscillation teleconnections. *Environmental Research Letters*, 9, 2014. URL http://iopscience.iop.org/article/10.1088/1748-9326/9/2/024014/pdf.

A. J. Charlton and L. M. Polvani. A new look at stratospheric sudden warmings. part i: Climatology and modeling benchmarks. *Journal of Climate*, 20(3):449–469, 2007. doi: 10.1175/JCLI3996.1. URL http://dx.doi.org/10.1175/JCLI3996.1.

G. P. Compo et al. The twentieth century reanalysis project. *Quarterly Journal of the Royal Meteorological Society*, 137(654):1–28, 2011.

D. P. Dee et al. The ERA-Interim reanalysis: configuration and performance of the data assimilation system. *Quarterly Journal of the Royal Meteorological Society*, 137(656):553–597, 2011.

J. W. Dungey. Interplanetary magnetic field and the auroral zones. *Physical Review Letters*, 6, 1961.

J. P. Eastwood, D. O. Kataria, C. R. McInnes, N. C. Barnes, and P. Mulligan. Sunjammer. *Weather*, 70(1):27–30, 2015. ISSN 1477-8696. doi: 10.1002/wea.2438. URL http://dx.doi.org/10.1002/wea.2438.

Freie Universität Berlin. The Quasi-Biennial-Oscillation (QBO) Data Serie. http://www.geo.fu-berlin.de/en/met/ag/strat/produkte/qbo/. Accessed: 2017-05-26.

Gelaro et al. MERRA-2- NASA's Modern-Era Retrospective Analysis for Research and Applications. *Journal of Climate*, 2016. Manuscript submitted.

Global Modeling and Assimilation Office (GMAO). MERRA-2 inst6_3d_ana_Nv: 3d,6-Hourly, Instantaneous, Model-Level, Analysis, Analyzed Meteorological Fields V5.12.4, 2015. Accessed: 24 May 2016.

L. J. Gray, J. Beer, M. Geller, J. D. Haigh, M. Lockwood, K. Matthes, U. Cubasch, D. Fleitmann, G. Harrison, L. Hood, J. Luterbacher, G. A. Meehl, D. Shindell, B. van Geel, and W. White. Solar influences on climate. *Reviews of Geophysics*, 48(4), 2010. ISSN 1944-9208. doi: 10.1029/2009RG000282. URL http://dx.doi.org/10.1029/2009RG000282.

P. Haynes. Stratospheric dynamics. *Annual Review of Fluid Mechanics*, 37(1):263–293, 2005. doi: 10.1146/annurev.fluid.37.061903.175710. URL http://dx.doi.org/10.1146/annurev.fluid.37.061903.175710.

J. R. Holton and H.-C. Tan. The influence of the equatorial quasi-biennial oscillation on the global circulation at 50 mb. *Journal of the Atmospheric Sciences*, 37(10):2200–2208, 1980. doi: 10.1175/1520-0469(1980)037<2200:TIOTEQ>2.0.CO;2. URL http://dx.doi.org/10.1175/1520-0469(1980)037<2200:TIOTEQ>2.0.CO;2.

IPCC. *Climate Change 2013: The Physical Science Basis. Contribution of Working Group I to the Fifth Assessment Report of the Intergovernmental Panel on Climate Change*. Cambridge University Press, Cambridge, United Kingdom and New York, NY, USA, 2013. ISBN ISBN 978-1-107-66182-0. doi: 10.1017/CBO9781107415324.004. URL www.climatechange2013.org.

E. Kalnay et al. The NCEP/NCAR 40-year reanalysis project. *Bulletin of the American Meteorological Society*, 77(3):437–471, 1996.

M. Kanamitsu et al. NCEP-DOE AMIP-II reanalysis (R-2). *Bulletin of the American Meteorological Society 83*, 83(11):1631–1643, 2002.

S. Kobayashi et al. The JRA-55 Reanalysis: General Specifications and Basic Characteristics. *Journal of the Meteorological Society of Japan*, 93(1):5–48, 2015.

P. Laloyaux, M. Balmaseda, D. Dee, K. Mogensen, and P. Janssen. A coupled data assimilation system for climate reanalysis. *Quarterly Journal of the Royal Meteorological Society*, 142(694):65–78, 2016.

M. L'Heureux, A. Butler, B. Jha, A. Kumar, and W. Wang. Unusual extremes in the negative phase of the arctic oscillation during 2009. *Geophysical Research Letters*, 37(10), 2010. ISSN 1944-8007. doi: 10.1029/2010GL043338. URL `http://dx.doi.org/10.1029/2010GL043338`. L10704.

H. Lu, M. J. Jarvis, and R. E. Hibbins. Possible solar wind effect on the northern annular mode and northern hemispheric circulation during winter and spring. *Journal of Geophysical Research: Atmospheres*, 113(D23), 2008. ISSN 2156-2202. doi: 10.1029/2008JD010848. URL `http://dx.doi.org/10.1029/2008JD010848`. D23104.

V. Maliniemi, T. Asikainen, K. Mursula, and A. Seppälä. QBO-dependent relation between electron precipitation and wintertime surface temperature. *Journal of Geophysical Research: Atmospheres*, 118:6302–6310, 2013.

J. Marshall and R. A. Plumb. *Atmosphere, Ocean and Climate Dynamics*. Elsevier, 2007.

R. J. Murgatroyd. The physics and dynamics of the stratosphere and mesosphere. *Reports on Progress in Physics*, 33(3):817, 1970. URL `http://stacks.iop.org/0034-4885/33/i=3/a=301`.

NASA Ozone Watch. What is a polar stratospheric warming? `https://ozonewatch.gsfc.nasa.gov/facts/warming_NH.html`. Accessed: 2017-05-04.

NOAA Earth System Research Laboratory. SSWC: Sudden Stratospheric Warming Compendium data set. `https://www.esrl.noaa.gov/csd/groups/csd8/sswcompendium/majorevents.html`. Accessed: 2017-05-26.

NOAA National Centers for Environmental Information. Geomagnetic kp and ap Indices. `https://www.ngdc.noaa.gov/stp/GEOMAG/kp_ap.html`, a. Accessed: 2017-05-30.

NOAA National Centers for Environmental Information. ENSO - What is it? https://www.ncdc.noaa.gov/teleconnections/enso/enso-tech.php, b. Accessed: 2017-05-17.

NOAA National Centers for Environmental Information. Arctic Oscillation (AO). https://www.ncdc.noaa.gov/teleconnections/ao/, c. Accessed: 2017-05-09.

K. Onogi et al. The JRA-25 reanalysis. *Journal of the Meteorological Society of Japan*, 85(3): 369–432, 2007.

R. A. Plumb. The interaction of two internal waves with the mean flow: Implications for the theory of the quasi-biennial oscillation. *Journal of the Atmospheric Sciences*, 34 (12):1847–1858, 1977. doi: 10.1175/1520-0469(1977)034<1847:TIOTIW>2.0.CO;2. URL http://dx.doi.org/10.1175/1520-0469(1977)034<1847:TIOTIW>2.0.CO;2.

J. P. Rafferty. Polar vortex. *Encyclopædia Britannica*, 2014. URL https://www.britannica.com/science/polar-vortex. Accessed: 2017-05-17.

M. M. Rienecker et al. MERRA: NASA's Modern-Era Retrospective Analysis for Research and Applications. *Journal of Climate*, 24(14):3624–3648, 2011.

E. Rozanov, L. Callis, M. Schlesinger, F. Yang, N. Andronova, and V. Zubov. Atmospheric response to NOy source due to energetic electron precipitation. *Geophysical Research Letters*, 32(14), 2005. ISSN 1944-8007. doi: 10.1029/2005GL023041. URL http://dx.doi.org/10.1029/2005GL023041. L14811.

S. Saha et al. The ncep climate forecast system reanalysis. *Bulletin of the American Meteorological Society*, 91(8):1015–1057, 2010.

W. Schwerdtfeger and F. Prohash. The Semi-Annual Pressure Oscillation, its Cause and Effects. *Journal of Meteorology*, 13(2):217–218, 1956. doi: {10.1175/1520-0469(1956)013<0217:TSAPOI>2.0.CO;2}. URL http://dx.doi.org/10.1175/1520-0469(1956)013<0217:TSAPOI>2.0.CO;2.

A. Seppälä and M. A. Clilverd. Energetic particle forcing of the northern hemisphere winter stratosphere: comparison to solar irradiance forcing. *Frontiers in Physics*, 2:25, 2014. ISSN 2296-424X. doi: 10.3389/fphy.2014.00025. URL http://journal.frontiersin.org/article/10.3389/fphy.2014.00025.

A. Seppälä, H. Lu, M. A. Clilverd, and C. J. Rodger. Geomagnetic activity signatures in wintertime stratosphere wind, temperature, and wave response. *Journal of Geophysical Research: Atmospheres*, 118:2169–2183, 2013.

A. Seppälä, K. Matthes, C. E. Randall, and I. A. Mironova. What is the solar influence on climate? Overview of activities during CAWSES-II. *Progress in Earth and Planetary Science*, 1(1):24, 2014. ISSN 2197-4284. doi: 10.1186/s40645-014-0024-3. URL http://dx.doi.org/10.1186/s40645-014-0024-3.

A. Seppälä, C. E. Randall, M. A. Clilverd, E. Rozanov, and C. J. Rodger. Geomagnetic activity and polar surface air temperature variability. *Journal of Geophysical Research: Space Physics*, 114(A10), 2009. ISSN 2156-2202. doi: 10.1029/2008JA014029. URL http://dx.doi.org/10.1029/2008JA014029. A10312.

A. K. Smith. Interactions between the lower, middle and upper atmosphere. *Space Science Reviews*, 168(1):1–21, 2012. ISSN 1572-9672. doi: 10.1007/s11214-011-9791-y. URL http://dx.doi.org/10.1007/s11214-011-9791-y.

Southwest Research Institute. Earth's Magnetosphere: Nature's Plasma Physics Lab. http://mms.space.swri.edu/science-4.html. Accessed: 2017-04-22.

D. W. J. Thompson. A Brief Introduction to the Annular Modes and Annular Mode Research. http://www.atmos.colostate.edu/~davet/ao/introduction.html. Accessed: 2017-05-09.

R. M. Thorne. The importance of energetic particle precipitation on the chemical composition of the middle atmosphere. *pure and applied geophysics*, 118(1):128–151, 1980. ISSN 1420-9136. doi: 10.1007/BF01586448. URL http://dx.doi.org/10.1007/BF01586448.

S. M. Uppala et al. The ERA-40 re-analysis. *Quarterly Journal of the Royal Meteorological Society*, 131(612):2961–3012, 2005.

I. G. Usoskin. A history of solar activity over millennia. *Living Reviews in Solar Physics*, 14 (1):3, 2017. ISSN 1614-4961. doi: 10.1007/s41116-017-0006-9. URL http://dx.doi.org/10.1007/s41116-017-0006-9.

Wikipedia. Arctic oscillation. https://en.wikipedia.org/wiki/Arctic_oscillation, a. Accessed: 2017-05-09.

Wikipedia. List of large volcanic eruptions of the 20th century. https://en.wikipedia.org/wiki/List_of_large_volcanic_eruptions_of_the_20th_century, b. Accessed: 2017-05-26.